https://doi.org/10.5194/egusphere-2025-2275
Preprint. Discussion started: 2 June 2025

The Carbon Mapper emissions monitoring system

Riley Duren[1], Daniel Cusworth[1], Alana Ayasse[1], Kate Howell[1], Alex Diamond[1], Tia Scarpelli[1], Jinsol Kim[1], Kelly O'neill[1], Judy Lai-Norling[1], Andrew Thorpe[2], Sander R. Zandbergen[2], Lucas Shaw[2], Mark Keremedjiev[3], Jeff Guido[3], Paul Giuliano[3], Malkam Goldstein[3], Ravi teja Nallapu[3], Geert Barentsen[3], David R.Thompson[2], Keely Roth[3], Daniel Jensen[2], Michael Eastwood[2], Frances Reuland[4], Taylor Adams[5], Adam Brandt[4], Eric A. Kort[5], James Mason[3], Robert O. Green[2]

[1]Carbon Mapper, Pasadena, 91105, USA
[2]Jet Propulsion Laboratory, California Institute of Technology, Pasadena, 91109, USA
[3]Planet Labs PBC, San Francisco, 94107, USA
[4]Stanford University, Stanford, 94305, USA
[5]University of Michigan, Ann Arbor, 48109, USA

Correspondence to: Riley Duren (riley@carbonmapper.org)

Abstract

The non-profit organization Carbon Mapper has a public good mission to drive greenhouse gas (GHG) emission reductions by making methane (CH_4) and carbon dioxide (CO_2) data accessible and actionable. The Carbon Mapper emissions monitoring system contributes to the broader ecosystem of greenhouse gas observations by locating and quantifying CH_4 and CO_2 super emitters at facility scale across priority regions globally. To meet these objectives, our system includes observing platforms, an operational monitoring strategy optimized for mitigation impact, and a data platform that delivers CH_4 and CO_2 data products for diverse stakeholders. Operational scale-up of our system is centered around a new constellation of hyperspectral satellites enabled by over a decade of sustained instrument technology and algorithm advances and prototyping with aircraft surveys and recent observations by NASA's EMIT instrument on the International Space Station. The Carbon Mapper Coalition (hereafter Tanager) satellites are each equipped with an imaging spectrometer instrument designed by NASA's Jet Propulsion Laboratory that are assembled, launched and operated by Planet Labs. The first Tanager satellite (Tanager-1) was launched 16 August 2024, completed commissioning in January 2025, and is on track for full operational monitoring by summer 2025. Planet is currently working to expand the constellation to four Tanagers. The system is designed to balance detection limits, spatial coverage and sample frequency to optimize observational completeness for high emission CH_4 and CO_2 point sources. Each imaging spectrometer instrument has a spectral range of about 400-2500 nm, 5 nm spectral sampling, a nadir spatial resolution of 30 meters, and nadir swath width of about 19 km. Each satellite is capable of imaging up to 300,000 km2 per day. By combining the results of independent controlled release testing with empirical evaluation of the radiometric, spectral, spatial performance, and retrieval noise performance of the Tanager-1 spectrometer, we predict minimum detection limits of about 66 – 144 $kgCH_4/h$ for CH_4 point sources and about 10,400 – 19,600 $kgCO_2/h$ for CO_2 point sources for images with 25% albedo, 45 degree solar zenith angle, and 3 m/s wind speed. Detection limit varies with imaging mode and environmental variables. Every Tanager satellite provides multiple imaging modes with varying degrees of ground motion compensation that allow trade-offs between detection limit and spatio-temporal coverage. The Carbon Mapper monitoring strategy focuses on routine mapping of major CH_4 and CO_2 emitting regions and priority facilities around the world. With a single Tanager satellite, the cloud-free median time to access ranges from 2 to 5 days for isolated areas of interest (AOIs) at mid-latitudes. With four Tanager satellites, the cloud-free median time to access is reduced to under 10 hours for isolated AOIs, with weekly to monthly sample frequency for comprehensive mapping of contiguous regions. The constellation is designed for scale-up by launching more satellites with an ultimate goal of providing routine sub-daily monitoring of all high priority regions and 90% observing system completeness for point sources. Additionally, the satellites are capable of sun-glint tracking over the ocean to allow monitoring of offshore oil and gas fields, a key emission sector that has largely gone unmonitored. A review of the first 7 months of Tanager-1 CH_4 and CO_2 observations including initial validation with coordinated aircraft under-flights and non-blind controlled release testing indicates that the system is meeting performance requirements and, in many cases, surpassing expectations. We also present early observational findings including the first use of Tanager data to guide the timely mitigation of a CH_4 super emitter.

https://doi.org/10.5194/egusphere-2025-2275
Preprint. Discussion started: 2 June 2025

1 Introduction and objectives

As governments, companies and actors across civil society pursue a broad range of efforts to stabilize and reduce greenhouse gas (GHG) emissions there is an increasing need for actionable emissions data that is accurate, timely, and trusted. The expanding portfolio of use-cases includes diverse governmental regulations, private sector market-based initiatives, leak detection and repair programs, and an increasing demand for measurement-based emission inventories and enhanced transparency. Example includes ambitious emission mitigation targets by governments under the Paris Agreement (UN 2015), Kigali Amendment (UN 2016), and Global Methane Pledge (UN 2023) as well as major private sector initiatives such as the Oil and Gas Methane Partnership (UNEP 2020). In parallel with these policy developments, dramatic advances in GHG measurement technology have occurred over the last several years – particularly for methane (CH_4) and carbon dioxide (CO_2), the top two climate pollutants.

Scaling up a global emissions monitoring system that can provide global operational tracking of millions of emission sources at facility-scale along with rapid, transparent data publication requires addressing technical as well as institutional barriers. To confront these challenges, the Carbon Mapper non-profit organization (https://carbonmapper.org/) was established with the support of philanthropists to provide leadership in observational system development, CH_4 and CO_2 science data analysis, and stakeholder engagement. We also assembled a public-private partnership called the *Carbon Mapper Coalition* to design and launch the first in a series of next generation satellites. The Carbon Mapper Coalition (hereafter Tanager-series) satellites are each equipped with an imaging spectrometer instrument designed by NASA's Jet Propulsion Laboratory (JPL) that are assembled, launched and operated by Planet Labs. Like existing hyperspectral research satellites (e.g., PRISMA, EMIT, and EnMAP), Tanager is multi-application ready. However, unlike those missions, for the sake of operational GHG monitoring globally, a large portion of Tanager's tasking capacity is allocated to mapping known CH_4 and CO_2 emitting regions or infrastructure. The first Tanager satellite (Tanager-1) was launched 16 August 2024, completed commissioning in January 2025, and is on track to begin full operational monitoring by summer 2025. In this paper we describe the design, observational strategy, and performance of the Carbon Mapper emissions monitoring system as enabled by a constellation of Tanager satellites.

1.1 Motivation and challenges for measuring and mitigating CH_4 and CO_2 point sources

Since 2005, the ability to quantify global GHG concentrations using backscattered solar radiance at various spatio-temporal scales has existed from space with atmospheric sounding satellites, which for CH_4 began with SCIAMACHY (Frankenberg *et al.,* 2011) and more recently GOSAT (Turner *et al.,* 2015) and the TROPOMI instrument onboard the Sentinel-5p satellite (Hu *et al.,* 2018). CO_2 measuring satellites include NASA's OCO-2 and OCO-3 missions (Crisp *et al.,* 2004; Eldering *et al.,* 2019) as well as GOSAT. The AIRS instrument onboard NASA's Terra satellite measures thermal radiance but is only sensitive to middle to upper tropospheric CH_4 (Zou *et al.,* 2016). These early generations of atmospheric sounding satellites –measure gas absorption features at sub-nanometer spectral resolution with high precision, but doing so requires coarse, multi kilometer-scale spatial resolution (Jacob *et al.,* 2022). These systems are optimized for quantifying the total CH_4 and CO_2 fluxes for a given region, including the net contributions of diffuse area sources (typically distributed over several kilometers) and condensed point sources (typically originating from surface features < 10 meters across). Therefore, detection and quantification for individual point sources from these instruments is only sometimes possible for very large sources whose emission are generally more than 50 t CH_4/h (Lauvaux *et al.,* 2021) or 1600 t CO_2/h (Nassar *et al.,* 2021). The regional flux mapping satellites have provided important constraints for atmospheric GHG budgets when their observations are assimilated with atmospheric chemistry and transport inverse models (e.g., Worden *et al.,* 2022, Byrne *et al.,* 2022). However, the spatial resolution of global inverse models is typically on the order of 25 - 400 km, which may be sufficient for regional flux quantification, but not identifying and quantifying individual point sources at the scale of meters or capturing the bulk of point source distributions. Past inverse modeling work has attempted to estimate facility-scale emissions for spatially isolated sources like individual landfills (e.g., Nesser *et al.,* 2024), but this requires temporal averaging, and even average emissions cannot be attributed to facility-scale for dense infrastructure regions like oil/gas fields or urban areas. More recently, MethaneSAT was launched in March 2024 and was designed to quantify both the total CH_4 emissions and larger point sources for global oil and gas production basins with higher spatial resolution than other regional flux mappers (Miller *et al.,* 2024).

https://doi.org/10.5194/egusphere-2025-2275
Preprint. Discussion started: 2 June 2025

Meanwhile, multiple studies have conclusively identified the existence of methane "super emitters" where a relatively small fraction of infrastructure is often responsible for a disproportionate fraction of total emissions from key regions and economic sectors. CH_4 super emitters have the potential for emission rates exceeding 100 kg/h and are often associated with point sources. Super emitters can be the result of leaks, malfunctioning equipment, or process venting – many of which can be temporary but, in some cases, may persist for months to years (Cusworth *et al*., 2024). Beginning in 2016 and 2017, members of our research team used advanced remote-sensing aircraft from JPL to conduct the first comprehensive, economy wide survey of methane emitters in California and found that less than 0.2% of the infrastructure is responsible for over a third of the state's entire methane inventory (Duren *et al.,* 2019). Since then, these intensive field campaigns have expanded to other key regions across the US and other jurisdictions and show that a relatively small fraction of facilities are responsible for 20-60% of total emissions spanning multiple economic sectors (Cusworth *et al.,* 2022; Sherwin *et al.,* 2024). Additionally, since 2020, Carbon Mapper aircraft surveys of California, Colorado, Pennsylvania, New Mexico and Texas have demonstrated that delivering actionable emissions data to facility operators and agencies can lead to expedited mitigation action (CARB 2022; CDPHE 2024). Participating operators have reported that roughly half of the methane emissions we identified at their facilities (primarily from oil and gas production, downstream natural gas and solid waste management sectors) are "fixable" and in a number of cases we have verified emission reductions with follow-up overflights. Another key finding is that many of these super emitters are highly intermittent, widely dispersed and difficult to find with conventional surface measurements that have limited coverage due to cost and logistical constraints [Cusworth *et al.,* 2021a].

Given the major contribution of super emitters to regional methane budgets and the opportunity they present for mitigation, tools are needed that can provide global monitoring of these large, dispersed and often transient sources. Aircraft and satellite instruments optimized for point source imaging can complement area flux mapping satellites by quantifying emissions from point sources at very high (1-30 meter) spatial resolution. Unlike area flux mapping satellites optimized for high spectral sampling over a narrow spectral range, many point source imagers tend to have coarser spectral sampling (5-10 nm) while being sensitive to the full Visible to Shortwave Infrared (VSWIR) spectral range of solar backscatter (e.g., 400-2500 nm) - which allows for a broader range of applications beyond trace gas sensing. Field campaigns with a class of VSWIR imaging spectrometers such as the next generation Airborne Visible/Infrared Imaging Spectrometer (AVIRIS-NG) and Global Airborne Observatory (GAO) have routinely shown that when flown at altitudes of 3 - 8km, single point source CH_4 emissions above 5-10 $kgCH_4/h$ for 3 m/s wind can be detected and quantified, and their plumes can be mapped with 3-8 m spatial resolution (Frankenberg *et al.,* 2016; Duren *et al.,* 2019; Cusworth *et al.,* 2021a). Those airborne instruments have also demonstrated the ability to quantify CO_2 point source emissions as low as about 8,000 $kgCO_2/h$ (Kim *et al.,* 2025) for a 3 m/s wind speed. The major benefit of such instruments is that their high spatial resolution can enable accurate attribution of observed CH_4 and CO_2 to plumes to specific emission sources at (and sometimes within) individual facilities. A key limitation of point source imagers is that they are primarily sensitive to discrete point sources rather than diffuse area sources and net emissions from regions. Another limitation of point source imagers is that singular instruments have limited spatio-temporal coverage, particularly aircraft surveys that are limited by logistics, cost and airspace restrictions. Individual point source imaging satellites can provide greater spatio-temporal coverage than aircraft but are still limited compared to regional flux mapping satellites. It is through the coordinated observations and analysis of data from point source imagers and regional flux mappers that truly complete, multi-scale understanding ofCH_4 and CO_2 emissions can be obtained, which we and others have demonstrated in previous studies (Cusworth *et al.,* 2022; Naus *et al.,* 2023).

1.2 Carbon Mapper monitoring system overview and objectives

Carbon Mapper has a public good mission to enable GHG emission reductions by making methane (CH_4) and carbon dioxide (CO_2) data more complete, actionable and accessible. We contribute to the emerging multi-scale ecosystem of global GHG observations by locating and quantifying CH_4 and CO_2 point sources at facility scale across key regions. While other programs are optimized for quantifying wide area methane emissions at the scale of regions and major oil and gas production basins, Carbon Mapper provides high resolution and high frequency tracking of methane and CO_2 emissions of individual facilities and pieces of equipment globally. Our primary objectives are to provide actionable mitigation guidance to facility owner/operators and regulators and improve awareness of emissions across civil society. Carbon Mapper data also can be integrated with other data sets to help evaluate and improve greenhouse gas inventories and accounting frameworks in support of the Global Methane

https://doi.org/10.5194/egusphere-2025-2275
Preprint. Discussion started: 2 June 2025

Pledge, Paris Climate Agreement, and mitigation targets of key sub-national jurisdictions. The Carbon Mapper emissions monitoring system is designed to fill critical gaps in the emerging global framework of greenhouse gas observing systems, providing actionable data at facility scale to drive leak repair efforts and hold emitters accountable. Stakeholders include US federal and state agencies and their counterparts in other countries, international data programs and registries, facility operators, development banks, non-governmental organizations, and civil society.

The Carbon Mapper emissions monitoring system includes observing platforms (Tanager satellites, aircraft , and EMIT), an operational monitoring strategy optimized for mitigation impact, and a data platform that delivers actionable, accessible, and transparent CH_4 and CO_2 data products for diverse stakeholders. Global scaling of this system is centered around the new constellation of Tanager satellites. The design of those satellites, along with Carbon Mapper's strategy for emissions monitoring and data platform were informed by nearly a decade of field campaigns and mitigation pilot projects using prototype aircraft sensors including the efforts in California, Colorado, New Mexico, and Pennsylvania.

2 System Design

Carbon Mapper's emissions monitoring system is motivated by an overarching goal to make CH_4 and CO_2 super emitters visible and to deliver data to guide efforts to mitigate (eliminate or reduce) them. The system design and operations are in turn driven by our priorities of maximizing completeness, actionability, and accessibility. We define completeness (also called Observing System Completeness) to be the percentage of a given population of emitters that can be detected based on an optimal balance of detection limits, spatial coverage and sample frequency (Jacob *et al.,* 2022). We define actionable to be timely data delivery and notification (e.g., latencies measured in hours and days rather than months) with precise and reliable geolocation and attribution of observed CH_4 and CO_2 plumes to specific emissions sources. We define accessible to mean that data is available to the largest possible set of stakeholders, is transparent and in formats that are readily understandable by a wide audience.

Carbon Mapper's monitoring strategy and the Tanager satellites are designed to optimize completeness. This metric constrains ultimate mitigation potential because characterizing a critical set of emitting infrastructure requires routine observation across large areas to identify specific leaks, equipment malfunctions and inefficient process venting. Actionability is the second major design driver. Using remote sensing to guide CH_4 leak detection and repair (LDAR) action requires that high emission events can be detected and reported quickly enough so that facility operators can verify and diagnose the root cause with follow-up site visits. Some super emitter events have the potential to eclipse the normal net annual emissions of an entire facility within a few days or weeks if not detected and repaired in a timely fashion (Pandey *et al.,* 2019). The Carbon Mapper emissions monitoring system is designed to deliver actionable information - images of emission plumes, estimated source coordinates, emission rate estimates, sectoral attribution - within 72 hours of each observation. The low latency capability is enabled by the Planet's small satellite platform that includes a high-speed downlink and backhaul capability combined with low latency data processing by the Planet and Carbon Mapper data platforms. The ability to precisely and reliably geolocate and attribute observed plumes to a physical emission source is critical both for effective support of LDAR programs and quantification of high emission activity at facility-scale. Another major design driver is data accessibility, where transparent availability of quality-controlled CH_4 and CO_2 emissions data is intended to provide maximum support for monitoring, reporting and verification programs, measurement informed inventories, and improved situational awareness for a diverse audience of stakeholders.

2.1 Emissions monitoring strategy

Mitigation potential is ultimately constrained by the fraction of emissions from a given population that can be observed. Our system is designed to provide sustained operational monitoring of the world's CH_4 and CO_2 super emitters at facility scale. In doing so, our program complements and leverages other key CH_4 and CO_2 observing systems, such as MethaneSAT, TROPOMI, GOSAT, OCO-2, OCO-3, etc., that provide critical insights into net regional emission fluxes including the contributions of diffuse area sources. At the same time, a key element of our strategy is scalability and continuity of the Tanager constellation which is strongly dependent on available financing for assembly, launch and sustained operation of the satellites. This is enabled by Planet's use of Tanager to support a broad portfolio of environmental indicators beyond CH_4 and CO_2 (e.g., various land surface variables) that are

https://doi.org/10.5194/egusphere-2025-2275
Preprint. Discussion started: 2 June 2025

derived from hyperspectral imaging across the full VSWIR spectral range. As a result, a large fraction of Tanager tasking capacity is allocated to observing known CH_4 and CO_2 emitting regions identified by Carbon Mapper and the remainder is allocated to either commercial CH_4 services, other hyperspectral applications, and/or maximizing coverage of land areas. A general operating rule for Tanager is to "always be imaging" – meaning the satellite will image targets of opportunity over land when not in conflict with other tasking priorities or completely overcast conditions. Regardless of which application motivates tasking of a given area, Carbon Mapper processes every Tanager image to quantify and publish any CH_4 and CO_2 emissions that are detected.

2.1.1 Completeness: maximizing mitigation potential

There are no formal specifications of super emitter populations that span all emission sectors and processes, but to guide our strategy we have established a reference distribution of emitters informed by empirical field campaigns, emission inventories, and analysis of Geographical Information System (GIS) datasets. For CH_4, we use findings from aircraft remote sensing surveys covering over half of US oil and gas production and over 250 landfills across multiple regions, jurisdictions, and time scales (Duren *et al.,* 2019, Cusworth *et al,* 2024). The aircraft measurement methods used in those studies typically offer a 90% probability of detection limit of 10-45 kg/h for 3 m/s wind speeds based on single-blind controlled release testing (El Abbadi *et al.,* 2024; Ayasse *et al.,* 2023). Additionally, a synthesis analysis combined nearly 1 million empirical measurements from those and other aircraft surveys with similar detection limits to construct a statistical model of all emissions > 0.1 kg/h for major US oil and gas basins and found that 20-80% of total emissions come from a relatively small population of sources emitting > 100 $kgCH_4/h$ (Sherwin *et al.,* 2024). Hence, we set 100 $kgCH_4/h$ as a reference definition for a CH_4 super emitter. The same threshold was adopted by the US Environmental Protection Agency's Super Emitter Program and Greenhouse Gas Reporting Rule for the oil and gas sector (US EPA 2024a; US EPA 2024b). Similarly, for CO_2, previous empirical studies and emission inventories indicate that 90% of fossil fuel power plant emissions come from plants emitting > 100,000 kgCO2/h (Cusworth *et al.,* 2021b). Hence, we adopt this as our definition of a CO_2 super emitter.

Effective emissions monitoring strategies rely on multiple variables and so to provide quantitative guidance for optimization, we apply the Observing System Completeness (C) metric, defined as the fraction of a reference population of emitters that can be detected by a constellation of satellites as a function of detection limit (C_D), spatial coverage (C_S), and temporal sampling (C_T) (Jacob *et al.,* 2022).

$$C = C_D \times C_S \times C_T \qquad (1)$$

C_D describes the fraction of a given population that exceeds the detection limit of the instrument and retrieval algorithms. C_D is constrained by spatial resolution and single measurement precision for a specified emissions distribution and set of observational conditions - primarily albedo, solar zenith angle, and wind speed. To achieve an optimal C_D we use the findings from the field studies described above to set a goal of 90% empirical probability of detection (POD) for point sources ≥100 kg/h for CH_4 and ≥100,000 kg/h for CO_2. A related approach for specifying detection limits is to define a Minimum Detection Limit (MDL) – a flux above which a detection could be considered confident. Historically MDL has been calculated analytically from the measurement noise based on key instrument parameters such as spectral, radiometric, and spatial performance. The simplicity of this calculation made it helpful in defining system requirements. Here, in contrast, our empirical POD standard is calculated from controlled release experiments. This makes it a more robust metric as it accounts for not just the instrument design on a per-pixel basis, but also the real-world imaging conditions with complications such as turbulence, surface clutter, and other effects that are difficult to model, along with the complete observational and analysis workflow. The empirical POC is more representative of the range of actual detection rate under real world conditions. However, it requires empirical evaluation of an as-built instrument and data analysis system spanning a range of emission rates using controlled release experiments and/or coordinated observations of a population of sources with independent measurement systems. We are currently working to establish an empirical 90% POD for Tanager methane data using a variety of methods which is anticipated to require a full year to collect enough coordinated observations. Meanwhile, to guide Tanager requirements during design and development we used airborne data collected from past field experiments to establish a linear relationship between the empirical 90% POD and analytical MDL following methods described by Ayasse et al., 2023. For a 90% empirical POD of 90 $kgCH_4/h$ we estimated an equivalent MDL of 63 $kgCH_4/h$ for Tanager's highest sensitivity imaging mode. That MDL target was used to set single measurement precision requirements and relate them to key instrument parameters such as spectral

https://doi.org/10.5194/egusphere-2025-2275
Preprint. Discussion started: 2 June 2025

sampling, SNR, and spatial resolution. In addition to instrument design, SNR also varies with environmental factors such as surface albedo and solar zenith angle, both of which in turn can vary with latitude and season. Our analysis and on-orbit validation of single measurement precision and MDL is described in section 4.

C_S describes the fraction of the spatial extent of a given population of emitters that is observed over a given time interval. To inform an observational "tasking deck" for the Tanager satellites we need to establish a prioritized set of locations and spatial extents of potential CH_4 and CO_2 point source emissions globally. This is important, because while each Tanager satellite is capable of imaging over 300,000 km^2/day, we cannot necessarily allocate all tasking capacity to observing CH_4 and CO_2 emissions (e.g., not every Tanager hyperspectral imaging opportunity is over a CH_4/CO_2 emission source) and we also need to balance spatial coverage with sample frequency. We use the following approach to inform the initial baseline Tanager CH_4 tasking deck. We start by defining the key global regions responsible for most of the world's CH_4 emissions from oil, gas, and coal production and use based on the spatially resolved (10 km grid) Global Fuel Exploitation Inventory (Scarpelli et al 2022). We filter to focus on the top 10 oil and gas producing countries and all signatories of the Global Methane Pledge – in each case identifying all known oil, gas and coal production emissions (we estimate contributing about 85% of fossil CH_4 emissions). We then add the locations of large known landfills and unmanaged waste dumps based on various global and national inventories, like the US Greenhouse Gas Reporting Program and the Climate Trace inventory. A representative CH_4 tasking deck resulting from this process is shown in Fig. 1. This is for illustration purposes and is subject to change. In this analysis we do not include a specific focus on CO_2 point sources however the CH_4 tasking deck described here envelopes the vast majority of fossil fuel power plants, refineries and other high emission CO_2 point sources.

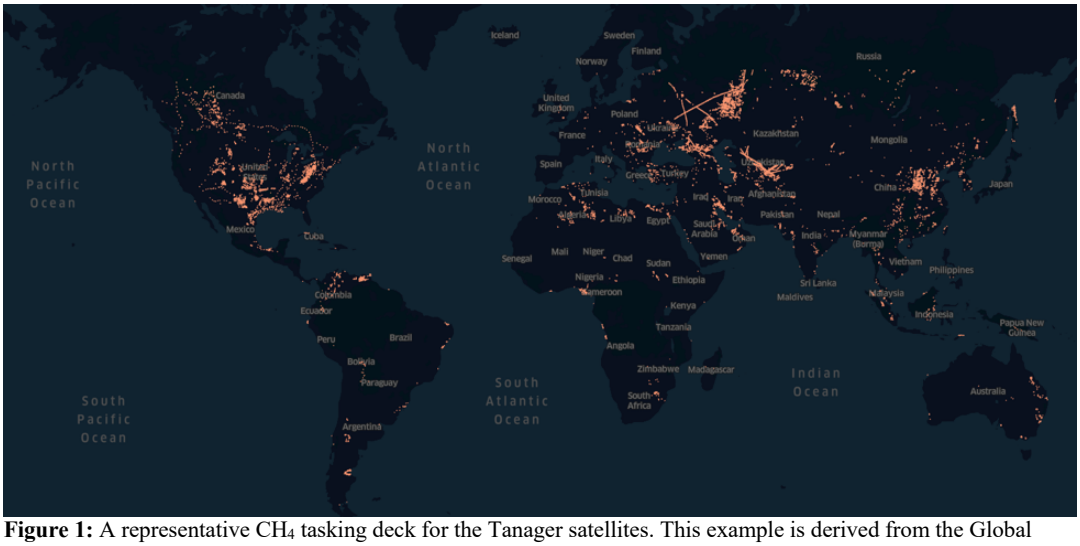

Figure 1: A representative CH_4 tasking deck for the Tanager satellites. This example is derived from the Global Fuel Exploitation Inventory and is predicted to cover 90% of global oil and gas (including onshore and offshore) and coal production emissions. The areas of interest here total nearly 1,000,000 km^2. Given the need for buffers and tasking overhead, Tanager satellites would need to image nearly 2,000,000 km^2 in total area to completely cover this tasking deck once. The map is subject to change based on evolving analysis of mitigation potential and other priorities. Not shown here are other key sectors such as waste management and agricultural operations or Tanager "background deck" imaging of land areas that are otherwise not actively prioritized for tasking.

C_T describes the likelihood that an emissions source above a given detection limit will be seen during a given interval as a function of the number of observations N, the source intermittency or frequency p (how often it is emitting above the detection limit), and the fraction of time F where the sky is clear over the emission source.

$$C_T = 1 - (1 - Fp)^N \qquad (2)$$

https://doi.org/10.5194/egusphere-2025-2275
Preprint. Discussion started: 2 June 2025

Temporal completeness and sample frequency are critical design considerations because CH_4 and CO_2 point source emissions are rarely static. Failing to account for variability and intermittency in monitoring system design can result in significant degradation in detection rates and completeness as well as biases in average emission estimates. Variability of CH_4 emissions over time can occur even for systems that are always "on" due to operational dynamics and changes in environmental conditions. For example, methane emissions from oil and gas production sites or landfills can vary dramatically over time scales of minutes to seasons in response to changes in oil production, gas pipeline pressures, or landfill gas collection rates and can also be influenced by ambient temperature, humidity, and atmospheric pressure. Additionally, some CH_4 sources are highly intermittent – meaning they can turn on or off completely at some duty cycle. Examples of intermittency include expected process emissions such as periodic pressure relief venting and normal venting from pneumatic devices such as compressors. Intermittency can also occur in situations involving leaking or malfunctioning equipment, for example in the case of unlit flares. Empirical field studies have characterized the distribution of intermittency in key sectors including oil and gas production and managed landfills (Duren *et al.,* 2019; Cusworth *et al.,* 2021; Cusworth *et al.,* 2024) and in some cases, a facility may have multiple sources with differing intermittencies like landfill flares versus the landfill work face (Scarpelli *et al.,* 2024). Based on these empirical studies, we use an assumed mean intermittency of 0.2 for oil and gas and 0.5 for landfill methane super emitters. Armed with intermittency constraints and cloud coverage statistics, we can then derive an optimal sample frequency of N observations per year that maximizes C_T and hence overall observing system completeness. We set an ultimate completeness target of 90% for CH_4 super-emitters $\geq$ 100 $kgCH_4/h$. Sample frequency is strongly constrained by the spatial distribution of the tasking deck and the number of satellites; however, we establish a mean sample frequency goal of 7 days for statistically complete monitoring of key regions. Additionally, we also set a goal of sub-daily sample frequency for high priority areas to better constrain the diurnal variability of many key processes including intermittent energy sector emissions.

2.1.2 Delivering actionable information

In the context of CH_4 and CO_2 information, we have leveraged nearly a decade of experience translating GHG data into action for diverse stakeholders to define "actionable" to mean data that is precise, timely, useful and reliable. Precise means sufficiently granular geolocation information to identify emission sources at the scale of individual facilities and sometimes major components within a facility. Precision can be important when it comes to attributing emission sources to economic sectors and equipment types. and it drives our observational requirements on spatial resolution, geolocation accuracy and data analysis. Timeliness means delivering data that is within the interest-horizon of a given stakeholder. For example, successful leak detection and repair programs at oil and gas facilities often rely on data from operational systems with latencies measured in hours and days rather than latencies of several months typical of research grade measurements. In some cases, facility operators may struggle to find an emission source if the latency between observation and notification is more than about 72 hours, particularly in cases with intermittently malfunctioning hardware. Additionally, delays of several days or weeks can translate to significant cumulative emissions from leaks that otherwise could have been mitigated quickly. Useful means data that is delivered in formats relevant to a stakeholder's priorities (e.g., towards guiding efficient operations or complying with regulatory requirements). Finally, reliable GHG information means data that is accurate, repeatable and trustworthy for a wide range of stakeholders. In turn, this drives requirements on thorough, well-documented quality control procedures, independent validation of Carbon Mapper data sets, and strategies to ensure continuity of the observational data record for many years. All these factors contribute to both the technical design of our observing systems, data platforms, stakeholder engagement programs, and the overall public-private partnership.

2.2 Instrument

Since 2016 our research team has used aircraft imaging spectrometers such as the Airborne Visible/Infrared Imaging Spectrometer (AVIRIS) series and Global Airborne Observatory (GAO) as well as research satellites to refine analysis methods and characterize CH_4 and CO_2 point source emissions from a range of sectors, resulting in the publication of over 15,000 CH_4 plumes to date (e.g., Thompson *et al.* 2015, Frankenberg *et al.* 2016, Duren *et al.* 2019, Cusworth *et al.* 2022, Thorpe *et al.* 2023, Cusworth *et al.* 2024) as well as initial CO_2 point source studies (Thorpe *et al.* 2017, Cusworth *et al.* 2023). Carbon Mapper has used AVIRIS-NG and GAO and, more recently, analysis of data from NASA's EMIT (Earth Surface Mineral Dust Source Investigation) instrument on the International Space Station (ISS) - to demonstrate the utility of this technique for actionable geolocation and quantification of methane point source emissions. However, none of those instruments were designed for greenhouse gas sensing. Deploying a truly operational point source imager in space with improved area coverage while minimizing CH_4 and CO_2 detection limits introduced some design challenges, e.g. the instrument must provide increased light gathering power without

https://doi.org/10.5194/egusphere-2025-2275
Preprint. Discussion started: 2 June 2025

sacrificing spectral sampling or spectral range. Preserving the full VSWIR spectral range rather than developing a spectrometer narrowly focused on the SWIR bands is necessary given the need to underpin the expansion and continuity of the Tanager constellation with commercial revenue for environmental data products that extend beyond CH_4 and CO_2 to serve a wide range of land and ocean hyperspectral applications.

Practically, this means that each Tanager imaging spectrometer instrument must have a detector sensitive to a wide spectral range, with large pixels which can efficiently collect many photons. It must also have a small focal ratio, or f-number, for maximum light-gathering power and high signal to noise ratio (SNR). It must have a fine spatial resolution, so that individual CH_4 or CO_2 emission plumes can be geolocated precisely enough for facility operators to quickly find and verify with follow-up site visits (e.g., within about 30 meters). The instrument must also have a sufficiently wide swath and along-track imaging capability to efficiently map large oil and gas production fields, major urban areas, and other priority regions for CH_4 and CO_2 point source emissions that can occur in a stochastic fashion. The key instrument parameters that resulted from these design trade-offs are summarized in Table 1. The swath width values shown here are for the final operational orbit altitude of 406 km; these values are ~30% higher during commissioning operations for a typical initial injection orbit of 510 km.

Table 1. Imaging spectrometer instrument specifications for a 406 km orbit altitude.

Parameter	Value
F-number	F/1.8
Focal Length	400 mm
Entrance Pupil Diameter	224.5 mm
Pixel Size	30 µm
Detector Array Size	640 x 480 pixels
iFOV	75.3 urad
Cross-track FOV	45.9 mrad
Swath Width	18.6 km (nadir) – 26.4 km (30 deg off-nadir)
Spectral Range	380 – 2500 nm
Spectral Sampling	5 nm
Spectral Response (FWHM)	≤6 nm
Spectrometer Temperature	250 K
Focal Plane Array Temperature	160 K
Radiometric Calibration Uncertainty	≤10%
Spectral Calibration Knowledge	5%
Spectral Cross-Track Uniformity	2%
Instrument mass	78 kg

The resulting Tanager instrument design leverages a rich history of previous imaging spectrometer development and refinement by the Jet Propulsion Laboratory over a period of more than 20 years, including instruments such as the Airborne Visible/Infrared Imaging Spectrometer (AVIRIS) series of airborne instruments, the Moon Minerology Mapper, and most recently, the EMIT instrument on the International Space Station. EMIT achieved first-light on 28 July 2022, with excellent uniformity and calibration, meeting all performance requirements (Thompson *et al.,* 2024). With a 60 meter spatial resolution, 7 nm spectral sampling, low inclination orbit and no ground motion compensation, EMIT is not optimized for greenhouse gas monitoring. However, EMIT has already provided a preliminary demonstration of CH_4 and CO_2 plume detection and quantification (Thorpe *et al.,* 2023) and Carbon Mapper's data platform has been routinely publishing those products to exercise workflow and quality control procedures in preparation for the Tanager satellites.

The Tanager instrument (Fig. 2) consists of a three-mirror anastigmat (TMA) telescope with a 22 cm aperture that focuses light at the slit of a Dyson spectrometer. The spectrometer consists of a lithographic slit, Dyson lens, grating, and focal plane array (FPA). The concentric Dyson spectrometer design offers higher optical throughput, with smaller footprint and lower mass than off-axis Offner spectrometers of similar performance (Mouroulis *et al.,* 2018). The spectrometer includes a CaF_2 glass Dyson lens and electron beam lithography-written diffraction grating on a concave, spherical substrate. The telescope mirrors are silver-coated and made from ultra-low expansion glass-ceramic material and are held strain-free via bipods attached to a carbon fiber composite optical bench assembly.

https://doi.org/10.5194/egusphere-2025-2275
Preprint. Discussion started: 2 June 2025

The telescope focuses light at the entrance slit of the spectrometer. In the spectrometer, the Dyson lens directs the light from the slit to the concave diffraction grating where the light is spectrally dispersed. From the grating, the first diffraction order light is directed back through the Dyson lens and focused onto the FPA after passing through an Order Sorting Filter (OSF), a three-zone bandpass filter that blocks unwanted grating orders. Straylight is minimized by the OSF, a zero-order light trap, and linear-variable anti-flection coating on the detector itself. The FPA is a substrate-removed Mercury Cadmium Telluride detector array with 640x480 pixels and 30 µm pitch that defines the 5 nm spectral sampling. There are 640 pixels in the cross-track (spatial) dimension and 480 pixels in the spectral dimension. The FPA has a full well of about 1 million electrons to maximize SNR for darker images while avoiding saturation for brighter images and provides high quantum efficiency and linearity with low readout noise. A cryocooler maintains the FPA temperature at 160 K to minimize dark current. A precision power supply unit and focal plane interface electronics minimize signal chain read noise in operating the FPA and providing analog to digital conversion. While the instrument can operate in a range of programmable integration times, the default value is ~8 ms (~ 125 frames per second). Digital instrument science data is sent to the spacecraft avionics for onboard storage and downlink.

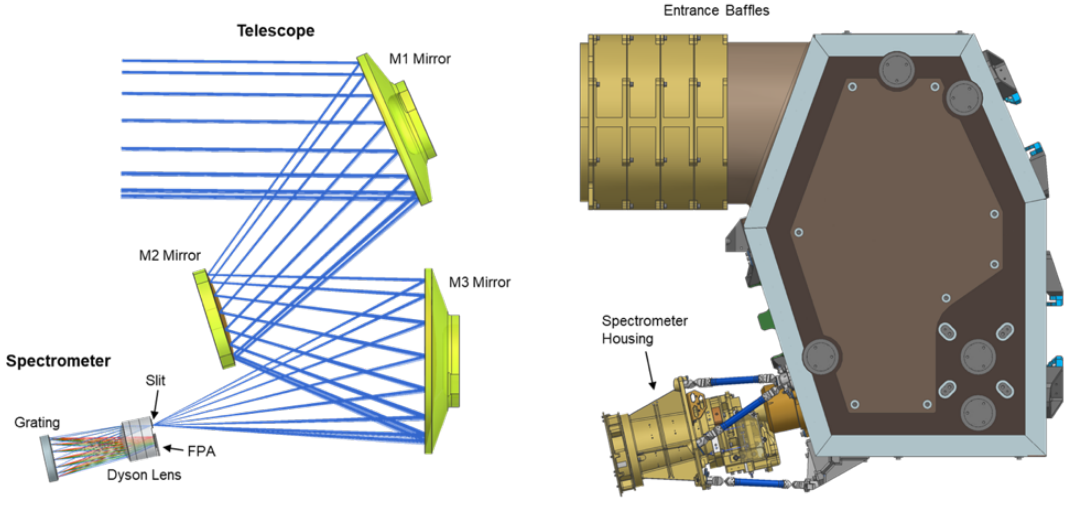

Figure 2. Tanager imaging spectrometer instrument. *Left*: Optical ray trace of telescope and the key Dyson spectrometer elements: slit, Dyson lens, grating, and Focal Plane Array (FPA). *Right*: the instrument optical bench assembly is composed of the entrance baffles, telescope housing, and Dyson spectrometer housing.

Instrument specifications are summarized in Table 1 and have been validated by a combination of lab tests and on-orbit measurements. The instrument design achieves excellent spectral uniformity, with keystone and smile each < 5%. [Zandbergen *et al.,* 2022] Optimal performance requires good radiometric and spectral calibration uncertainty which the instrument design constrains to <10%. The optics and baffling provide out of field stray light rejection by limiting detector illumination from extended field light sources to less than or equal to 10% of the input image irradiance. Each instrument has a 2.589 degree usable cross-track field of view (FOV) and 75.3 micro-radian cross-track instantaneous FOV (iFOV), translating to an approximately 19 km wide swath at nadir (up to 26 km with 30 deg off-nadir viewing) at the target science altitude of 406 km. Note that the swath width is initially nearly 30% larger during commissioning operations due to the higher injection orbit, typically around 510 km. The instrument spectral range is about 380 to 2500 nm with 5 nm spectral sampling set by the focal plane array size and spectrometer design. The spectral response function is iteratively tuned during/after instrument cold alignment testing and the verified on-orbit median values for Tanager-1 are 6 nm full-width half-maximum (FHWM) across the spectral range, approaching the 5 nm sampling in the critical SWIR bands (Fig. 3). The spectrometer is optimized for high SNR, particularly in the CH_4 absorption band between 2100 and 2430 nm (Fig. 4).

https://doi.org/10.5194/egusphere-2025-2275
Preprint. Discussion started: 2 June 2025

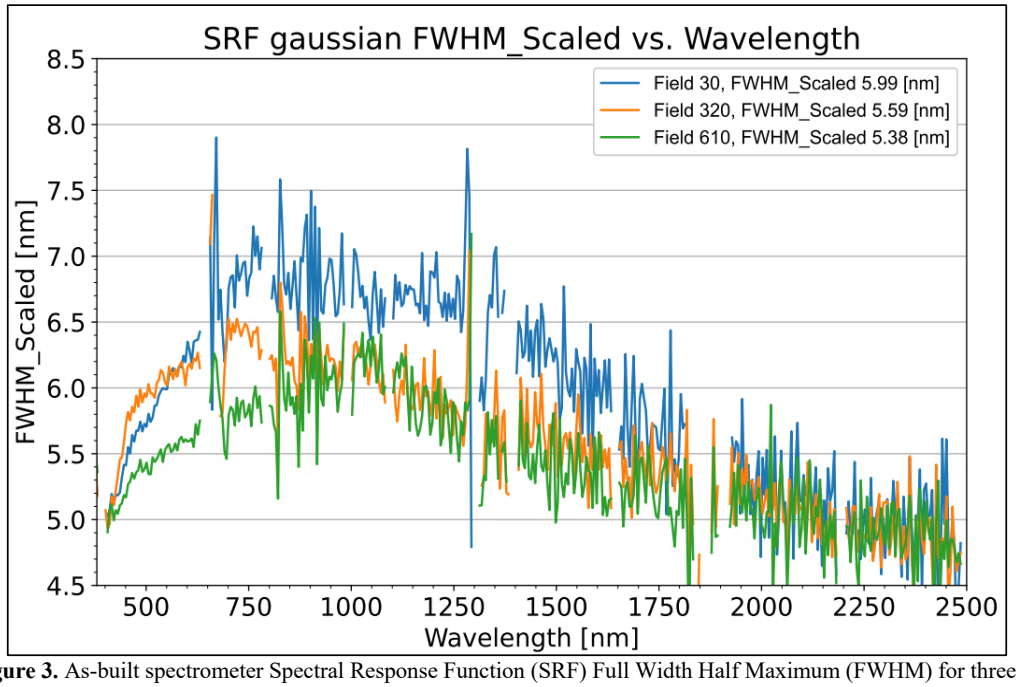

Figure 3. As-built spectrometer Spectral Response Function (SRF) Full Width Half Maximum (FWHM) for three columns spanning the cross-track direction based on lab testing with a monochromator. The average SRF approaches the spectral sampling of 5 nm in the critical SWIR bands for CH_4 and CO_2 retrievals (1960-2430 nm). For reference, the SRF for EMIT is approximately 8.5 nm FWHM.

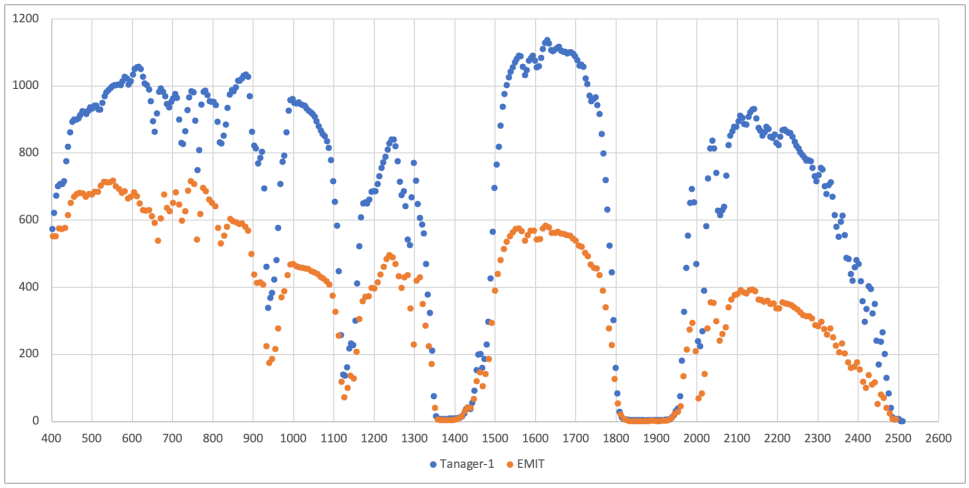

Figure 4. As-built spectrometer SNR across the full spectral range for Tanager-1 instrument compared with EMIT for reference. The Tanager values are for maximum sensitivity imaging mode (four stacked 8 millisecond exposures) and a 30 deg off-nadir viewing angle. EMIT is limited to nadir imaging (single 4 millisecond exposures). Both plots are for the same reference radiance with 35 deg solar zenith angle and 25% surface albedo. Note the significantly higher Tanager SNR compared to EMIT in the key 2300 nm CH_4 retrieval band, enabled by Tanager's ground motion compensation capabilities.

https://doi.org/10.5194/egusphere-2025-2275
Preprint. Discussion started: 2 June 2025

2.3 Tanager Smallsat Platform

Planet's Smallsat Platform includes a common satellite bus (Fig. 5), designed, manufactured, integrated, and tested in-house at Planet HQ. This common bus design is used by both Planet's Pelican and Tanager (Carbon Mapper Coalition) constellations. The first Smallsat Platform satellite was sent to space in November 2023 with the launch of Pelican-1, Planet's technology demonstration for its next-generation, high-resolution satellite fleet. This was followed in January 2025 with the launch of Pelican-2. In addition to the satellite bus, the Smallsat Platform includes Planet's global network of ground stations, mission control, and autonomous mission operations - making it interoperable with the entire Planet infrastructure.

Figure 5. Artist rendering of a Tanager satellite carrying the hyperspectral imaging spectrometer instrument. Courtesy: Planet Labs PBC.

The Smallsat Platform combines performance aspects of Planet's Dove satellites and SkySat constellation. It is modular, flexible, and extensible, and is compatible with multiple launch providers. The Smallsat Platform bus include a 600W power system, a high agility platform that can hold arc-second pointing accuracy and stability, multiple space qualified processors including state-of-the-art Field Programmable Gate Arrays (FPGAs), Graphics Processing Units (GPUs) and 2 Terabytes (TBs) of onboard storage capacity, low and high speed communication busses (CAN, Ethernet, SpaceFiber, PCIe), TT&C radio, high speed uplink and downlink radios, and advanced features such as real time intersatellite-link connectivity and an onboard Edge compute platform. This platform is interoperable with the entire Planet infrastructure from order management to ground operations to imagery pipeline and analytics.

With a peak downlink rate of up to 10Gbps, each Tanager satellite is designed to be able to downlink at least 250 Gigabytes per day of hyperspectral data on average via a flexible global ground network. This data is backhauled from Planet's globally distributed ground stations to Planet's cloud platform for image processing, insight extraction, and dissemination including to Carbon Mapper's data platform. Four Ka-band ground stations are already operational and actively supporting Tanager-1 and Planet's Pelican satellites. Table 2 summarizes the Tanager Smallsat Platform specifications.

https://doi.org/10.5194/egusphere-2025-2275
Preprint. Discussion started: 2 June 2025

Table 2. Tanager smallsat platform specifications

Parameter	Value
Orbit type	Sun Synchronous Orbit
Operational orbit altitude	406-430 km
Local Time of Descending Node	1100-1300 at the equator
Platform mass	200 kg (including 80 kg payload)
Design lifetime	5 years
Power (end of life)	600W generation, 650 Whr storage, 32V bus
Communications	S/X-band telemetry, tracking, command S-band high speed upre (512 kbps) Ka-band high speed downlink (10 Gbps)
Security	AER256 encryption on TT&C and imagery Link layer encryption on high speed downlink
Avionics/compute/storage	Space qualified processors, FPGAs, GPUs 2 Terabytes onboard storage
Guidance, Navigation, Control	<10 arcsec pointing accuracy 15 deg/sec slew rate Solar electric propulsion Dual band GPS receivers

2.4 Orbit and Imaging Modes

Each Tanager satellite is launched into a near polar Sun Synchronous Orbit (SSO) with a goal of achieving an optimal local time of the descending node (LTDN) or crossing time at the equator between 1100 and 1300 hours. This ensures consistent and maximum daylight illumination for spectroscopic observations. The initial injection altitude varies by individual launch but is typically around 510 km. Each Tanager satellite uses electric propulsion to maneuver to the final operational altitude of 406 km during commissioning and then maintains operational altitude over the 5-year design life. For example, Tanager-1 was launched into an initial 510 km altitude orbit with an initial LTDN of approximately 1040 hours. Tanager-1 was subsequently maneuvered into an interim orbit with a 430 km average altitude by January 2025 with a goal to complete maneuvering to the target 406 km and 1200 LTDN. The final orbit parameters are selected to provide an optimal balance between SNR, spatial resolution, FOV and global access. By deploying multiple satellites with differing orbital planes and crossing times we can better constrain the variability and intermittency of emission sources.

The observing geometry of each Tanager satellite is described in Fig. 6. The imaging spectrometer is a pushbroom sensor where the image swath width is set by the instrument iFOV, 640 cross-track (spatial) elements of the focal plane, and the degree of off-nadir pointing. Our primary observing strategy leverages the agility of the Tanager satellites to provide cross-track imaging of strips, nominally up to $\pm$ 30 degrees left or right of the nadir ground track. This is done by rolling the satellite to a fixed off-nadir angle prior to imaging. The length of each image is set by the imaging mode.

As summarized in Fig. 7 and table 3, Tanager offers four standard imaging modes ranging from 1 to 4 exposures per surface footprint. Tanager satellites offer ground motion compensation (GMC) by back-nodding in the along-track direction to offset the orbital rate during an image exposure. This prevents along-track pixel stretch while enabling multiple exposures of a surface footprint. Since the instrument is shot noise limited, the effective SNR scales with $\sqrt{N}$ where N is the number of exposures. For example, using the instrument standard 8 millisecond integration time per exposure, GMC allows up to 4 exposures to be acquired of the same surface footprint, where image stacking results in an effective integration time of about 32 ms and SNR about twice that of a single 8 ms exposure. Increasing the number of exposures increases SNR at the expense of decreasing along-track strip length and hence image area. Single image areas range from 346 to 8,700 km^2. This provides flexibility for trading off detection limit versus area coverage when designing an observing strategy for a given region, emission sector, or stakeholder use-case. Similar to EMIT and other airborne and satellite imaging spectrometers (but not shown in Fig. 7), the Tanager satellites are also capable of operating in pure nadir-viewing push-broom mode that allows image captures as long as

https://doi.org/10.5194/egusphere-2025-2275
Preprint. Discussion started: 2 June 2025

1080 km but doing so results in pixels that are 60 meters along track, with lower effective SNR, and less efficient sampling.

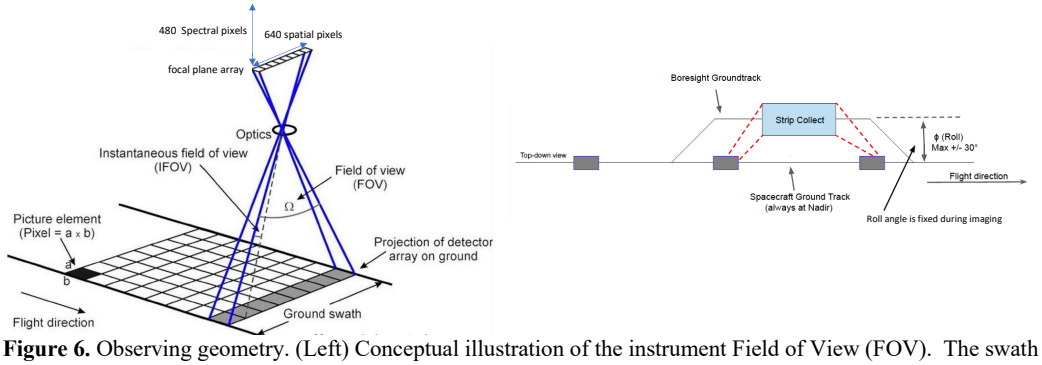

Figure 6. Observing geometry. (Left) Conceptual illustration of the instrument Field of View (FOV). The swath width is set by the focal plane array's 640 cross track spatial pixels projected onto the earth below the satellite. The spectrometer disperses light across the 480 spectral pixels in each line as the satellite forward motion images the earth. (Right) Top-down view illustrating Tanager's ability to roll in the cross-track direction (nominally up to ± 30 degrees) to image strips to the left or right of the nadir ground path.

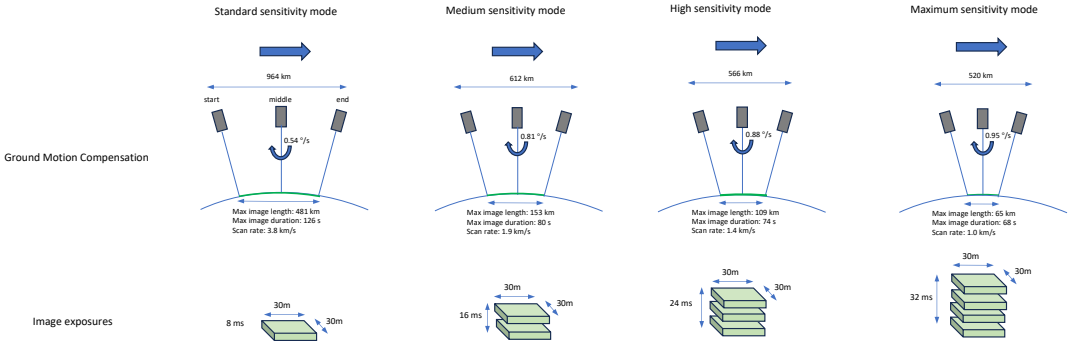

Figure 7. Tanager standard imaging modes. For each mode, the Tanager satellite back-nods with a given angular rate to provide ground motion compensation. The top part of the figure indicates satellite orientation at the start, middle and end of an image acquisition. The bottom part of the figure indicates the footprint of a single pixel for the specified number of 8 millisecond exposures. The range of imaging modes provides flexibility to trade between along-track spatial coverage and effective integration time for each image by selecting varying degrees of ground motion compensation. From left to right: standard sensitivity (single exposure) with 481 km maximum image strip length, medium sensitivity (two stacked exposures) with 153 km maximum strip length, high sensitivity (three stacked exposures) with 109 km maximum strip length, and maximum sensitivity (4 stacked exposures) with 65 km maximum strip length. Single image areas range from 346 to 8,700 km^2 and the along-track spatial resolution is preserved in each of these modes.

https://doi.org/10.5194/egusphere-2025-2275
Preprint. Discussion started: 2 June 2025

Table 3. Summary of integration time, spatial coverage, and SNR in the 2300 nm methane band (assuming a 25% albedo and 35 degree solar zenith angle) for the primary imaging modes. For each mode, area coverage is adjustable by selecting the along-track image length. Standard (1x8) imaging mode is planned for most ocean glint observations however the maximum image area will typically be constrained by the size of the sun glint spot.

Imaging Mode (Sensitivity)	N samples x Integration time (ms)	Minimum Area per Image (km2)	Maximum Area per Image (km2)	SNR at 2300 nm
Maximum	4 x 8	346	1209	615
High	3 x 8	346	2027	532
Medium	2 x 8	346	2846	435
Standard	1 x 8	346	8947	307

Given that 30% of global oil and gas production occurs in offshore environments any complete monitoring system must be capable of assessing emissions from production platforms, drilling ships and related infrastructure. Previous aircraft studies indicate that the magnitude, intensity and persistence of CH_4 emissions in some offshore environments exceed what is routinely seen in onshore production (e.g., Biener *et al.,* 2024, Gorchov Negron *et al.,* 2023, Ayasse *et al.,* 2022). Tanager satellites are designed to conduct sun-glint observations over the ocean (Fig. 8). This is critical for detecting methane emissions from offshore oil and gas platforms and potentially tanker vessels given that the ocean is dark at SWIR wavelengths. Aircraft prototyping indicates that sufficiently agile platform pointing and advance planning can align the instrument line of site with the bright specular sun-glint spot and infrastructure of interest (Ayasse *et al.,* 2022). Tanager sun-glint observations typically use Standard imaging mode. The number of imaging opportunities for ocean glint spots is more restricted than for land observations given the need to align the sun-glint spot over areas of interest. For example, a maximum duration land observation in Standard imaging mode is 126 seconds or 481 km along track but most sun-glint observations will be limited to about 14 seconds on average or 53 km along track (Nallapu *et al*., 2022). While Tanager-1 is demonstrating the successful application of sun-glint observations, we have not yet transitioned to operational offshore mapping.

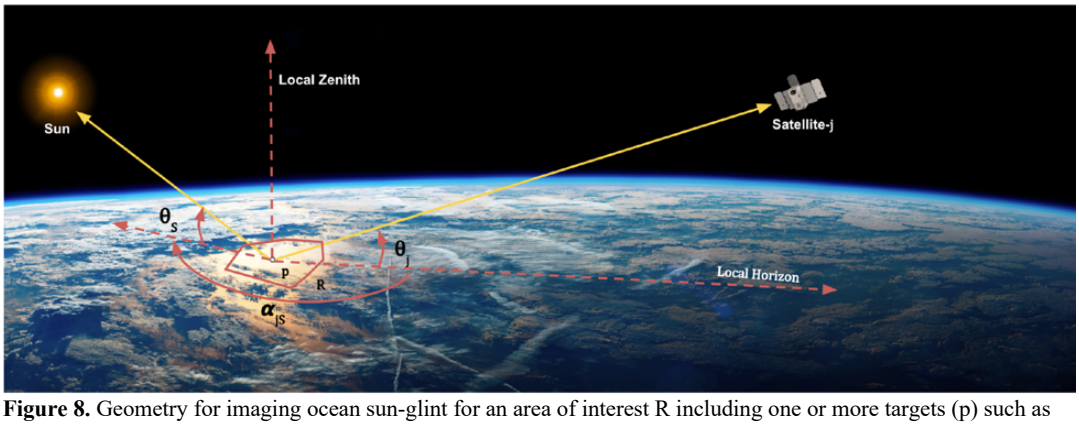

Figure 8. Geometry for imaging ocean sun-glint for an area of interest R including one or more targets (p) such as offshore oil and gas platforms. Tanager sun-glint observations typically use Standard (1x8 ms) imaging mode. Background image courtesy NASA.

Following launch, each Tanager satellite undergoes a commissioning phase that lasts several months and includes activation and checkout of spacecraft and instrument subsystems, a first light campaign to evaluate initial spectrometer performance at the injection altitude, followed by several months of propulsive maneuvers into the final lower orbit where calibration and validation efforts are completed prior to transition into steady state operations.

https://doi.org/10.5194/egusphere-2025-2275
Preprint. Discussion started: 2 June 2025

2.5 Data platforms and products

The focus here is on data processing applied to Tanager observations however the same basic procedures for generating calibrated radiance (Level 1) products are applied to the aircraft and EMIT observations used by the Carbon Mapper emissions monitoring system. Carbon Mapper retrievals, plume detection, emission estimation and quality control procedures are also uniformly applied to Tanager, EMIT and aircraft data to generate Level 2 – 4 CH_4 and CO_2 data products. Figure 9 summarizes the operational data analysis workflow for CH_4 and CO_2 emissions.

2.5.1 Level 1 processing

For Tanager observations, Planet's data platform generates the Level 1 data product that consists of georectified radiance files that are delivered to Carbon Mapper's data platform for retrieving CH_4 and CO_2. This process begins with Planet's data platform receiving raw data from the Tanager satellites via the Smallsat Platform high speed downlink and backhaul. The raw images are first orthorectified using a combination of digital elevation data and a full state model that is iteratively refined using a set of globally distributed ground-controlled points derived from reference imagery (e.g., Landsat 8). The combination of this approach with pointing telemetry from the spacecraft enables rectification accuracy well below the 30 meter (CE90) requirement.

Planet conducts pre- and post-launch calibration of each payload to quantify spectral, radiometric, spatial and uniformity characteristics. The calibration and characterization of the Tanager instruments is based on procedures developed by JPL that have been refined and proven over more than 30 years including those successfully demonstrated with the AVIRIS series of airborne instruments and the EMIT mission (Thompson *et al.* 2024). These procedures allow raw sensor digital numbers (DN) to be converted to physical sensor units. The result is a calibrated Top Of Atmosphere (TOA) radiance hypercube for each image. Additionally, the Planet data platform generates a cloud mask to support Level 2 processing.

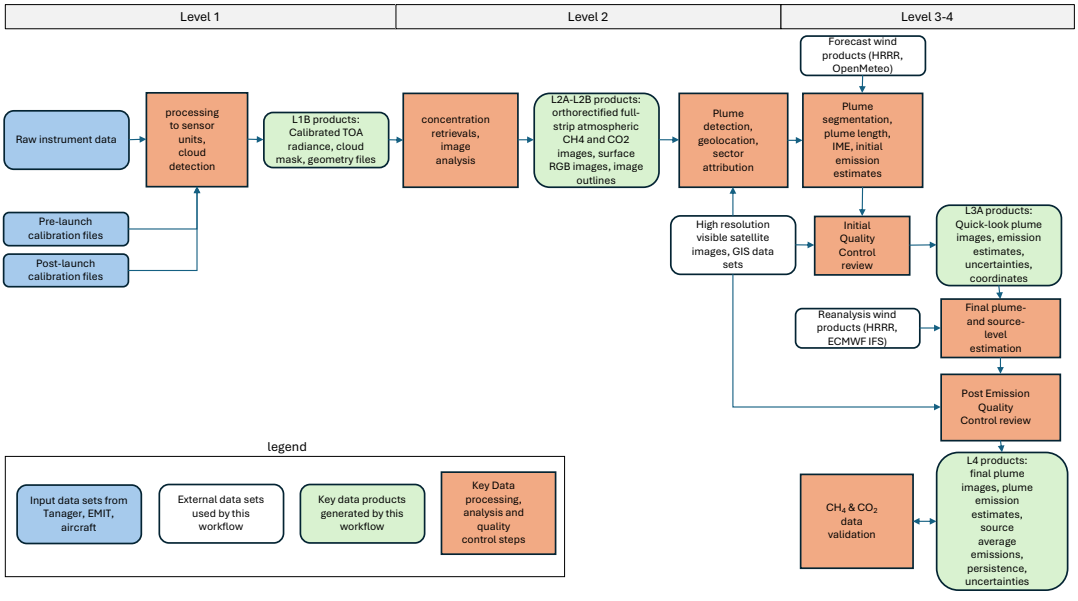

Figure 9. Carbon Mapper data analysis workflow applied to Tanager, EMIT and aircraft observations.

Pre-launch calibration is conducted in a thermal-vacuum chamber to mimic on-orbit conditions, with optical subsystems (telescope, spectrometer, and detector) held at the midpoints of the allowable flight temperature

https://doi.org/10.5194/egusphere-2025-2275
Preprint. Discussion started: 2 June 2025

performance ranges, within required thermal stability specifications (Zandbergen, *et al.* 2023). Each Tanager instrument undergoes the following pre-launch calibration testing program, including radiometric parameters measured with a National Institute of Standards and Technology (NIST) lamp and panel.

Spectral
- Spectral Range, Spectral Sampling, Spectral Calibration Knowledge
- Spectral Response (SRF)

Spatial
- Spatial Sampling - Broadband Slit
- Cross-track Spatial Response Function (CRF)
- Along-track Spatial Response Function (ARF)
- Slit (Camera) Model

Uniformity
- Spectral Cross-track Uniformity (smile)
- Spectral IFOV Uniformity (keystone)

Radiometric
- Radiometric Range (maximum reflectance)
- Radiometric Calibration Uncertainty
- Signal-to-Noise Ratio
- Swath Width

Stray Light
- In-field Spectral Scatter
- In-field Spatial Scatter
- Specular Ghosts

These in-lab measurements verify that the instruments meet the mission requirements and are used to generate initial calibration files. These files are an integral part of our data processing pipeline, allowing conversion of instrument Digital Numbers (DNs) to accurate physical units of radiance pre-launch.

On-orbit, each Tanager regularly collects dark field calibration data, flat fields, and monitors for saturated pixels/bad pixels. Planet monitors each Tanager instrument Focal Plane Array's (FPA) drift in dark bias by frequent acquisition of "dark fields" throughout the satellite's life. Dark field collections are tasked automatically once per orbit. We use the Earth-facing acquisition strategy currently used by EMIT, imaging over regions specified in their existing dark ocean map. Multiple frames are acquired in a single dark field acquisition and are analyzed to identify and drop outliers, then aggregated to form a single dark bias estimate for use in subsequent image processing to correct the bias. Images are processed with their most recent dark field which are planned to meet Planet's quality standards.

Additionally, the flat field can change on orbit across multiple spatial and temporal scales. Over short timescales, electronic drift in the amplifier and readout circuits can alter the sensitivity of distinct FPA elements and columns (e.g., due to temperature fluctuations or electromagnetic interference). Over longer periods, physical degradation or contamination of optical components can result in broader spatial changes. As a result, we monitor and update the laboratory flat field on orbit, both to support calibrated radiance data processing and to facilitate on-orbit instrument performance monitoring. As a baseline strategy, we collect flat fields over well-known calibration sites (i.e., PICS) on a monthly basis. These are acquired using standard collection modes as well as Side-Slither mode. Side-Slither mode enables the instrument to collect frames in a 90 degree rotation, making along-track movement aligned with cross-track elements. This determines that each element of the FPA covers the same area on the ground.

The above process uses many of the scientific algorithms used in the NASA EMIT Science Data System, including the ISOFIT atmospheric correction algorithms (Thompson et al., 2018). These algorithms and associated code are openly available in GitHub and maintained by JPL.

https://doi.org/10.5194/egusphere-2025-2275
Preprint. Discussion started: 2 June 2025

During the 4 months following activation and checkout of the Tanager-1 spacecraft and instrument subsystems, a full scientific validation of instrument calibrations and calibrated radiance products was completed by Planet and JPL. Tanager satellites image a range of regularly used calibration/validation sites (e.g., RadCalNet, PICS), including those instrumented to collect coincident ground and atmospheric data. Initial calibration assessments based on in-lab measurements and adjustments (e.g., band wavelengths and radiometric calibration coefficients) have been made. The team also orchestrated a ground calibration campaign at Ivanpah Playa, California, in March 2025. Ground teams used field spectrometers to measure surface spectral reflectance and upward-looking sensors to measure surface solar irradiance and estimate atmospheric properties. Using procedures described by Bruegge *et al.* (2021), we can predict Tanager at-sensor radiance to validate and update the radiometric calibrations for the satellite. A more comprehensive description of Tanager-1 spectrometer calibration will be published in a future paper.

2.5.2 Level 2 processing

For Tanager observations, the Carbon Mapper data platform uses calibrated radiance files delivered by Planet to derive several Level 2 data products. The L2 image outline products are the geographic boundaries, or "strips" of areas imaged by the Carbon Mapper Coalition satellites. Strip image outlines are helpful for determining where data is collected, the quality of that data, and verifying when methane or carbon dioxide sources are imaged, but no emissions above our detection limit were observed. In optimal observing conditions, such as an unobstructed view of the emission source and a high likelihood of detection, the absence of detection is termed a "null detect." The null detects imply that the source is not emitting methane above the sensor's minimum detection limit. We consider an image to be a good candidate for a null detect status for an emission source if the image contains less than 25% cloud cover and intersects any of the plume origin points estimated for the source. All Tanager L2 products are resampled to 30 meter resolution.

L2A Reference basemap images

L2A products are three-band (red-green-blue), natural color images of the Earth's surface generated from Tanager radiance files. This process involves correcting for atmospheric effects, geometric distortions, and terrain variations to produce accurate and visually appealing representations of the Earth. Carbon Mapper's operational workflow includes the use of Planet's Planetscope 5 meter resolution visible band images that are updated globally on a monthly cadence. In cases where Tanager's 30 meter spatial resolution is not sufficient to clearly identify the sector/facility type, Carbon Mapper may request high resolution (< 1 meter) visible band tasking from Planet's SkySat satellites. Carbon Mapper analysts use the various visible band image products and GIS data sets to help support attribution of observed CH_4 and CO_2 plumes to specific emission sectors, facilities, and, where possible, equipment types.

L2B Atmospheric retrievals

L2B products consist of orthorectified full-strip atmospheric retrieval images derived by the Carbon Mapper data platform from L1B calibrated radiance files to retrieve column or concentration length CH_4 enhancements (units ppm-m) in the strong methane SWIR band between 2200-2400 nm and concentration length CO_2 enhancements between 1900-2100 nm. We use algorithms that build on experience gained from previous airborne surveys with the AVIRIS-NG and GAO imaging spectrometers and analysis of EMIT data.

Column-wise Matched Filter

The column-wise matched filter (CMF) algorithm seeks an estimate for concentration length enhancement of CH_4 or CO_2 ($\hat{\alpha}$) for each observed spectrum (Thompson et al., 2016; Thompson et al., 2015). This is done by testing each observed spectrum against a target signature ($\vec{t}$), accounting for noise and background covariance $\mathbf{\Sigma}$. At sensor radiance $\boldsymbol{L_m}$ (unit μW/cm/sr/nm) for a pixel affected by enhanced gas concentration is modeled through Beer-Lambert's Law:

$$\boldsymbol{L_m = L_o e^{-k\alpha}} \quad (1)$$

https://doi.org/10.5194/egusphere-2025-2275
Preprint. Discussion started: 2 June 2025

Where $\boldsymbol{L_0}$ represents at-sensor radiance in presence of background levels of a gas, and $\vec{k}$ represents gas absorption. This model can be further simplified using Taylor expansion, assuming an optically thin plume:

$$\boldsymbol{L_m \approx L_o - \alpha t(L_o)} \quad (2)$$

Where $\boldsymbol{t(L_0) = k * L_0}$, the unit absorption spectrum, as is calculated through radiative transfer simulations of transmittance. To estimate $\boldsymbol{L_0}$, we use the mean spectrum $\boldsymbol{\mu}$ for all pixels in a "column" (i.e., all pixels in the flight direction of a single cross-track element) of observed data:

$$\boldsymbol{L_m \approx \mu - \alpha t(\mu)} \quad (3)$$

The optimal value of the concentration length, $\hat{\alpha}$, is found through optimization of log-likelihood - e.g., for the *i*th spectrum, $\hat{\alpha}_i$ is the solution that minimizes the residual between observed and modeled spectra while accounting for covariance. The maximum likelihood solution takes the following form (Foote et al., 2021):

$$\hat{\alpha} = \frac{\boldsymbol{t^T \Sigma^{-1}(L_m - \mu)}}{\boldsymbol{t^T \Sigma^{-1} t}} \quad (4)$$

The covariance matrix $\boldsymbol{\Sigma}$ is estimated from these same pixels in the along-track column. We employ a low-rank approximation for covariance to stabilize the solution in Equation 4, especially under regimes of few pixels per column (Thompson *et al.* 2015; Manolakis *et al.* 2009)

We follow the approach described in Foote et al., (2021) and select an image-specific unit absorption for each observation for both retrievals of CH_4 and CO_2 that depends on water vapor, ground elevation, and solar zenith angle. For column water vapor content, for each image acquisition, we query either the High Resolution Rapid Refresh (HRRR) meteorological product in the U.S. or the European Centre for Medium-Range Weather Forecasts European Centre for Medium-Range Weather Forecasts (ECMWF) Integrated Forecast System (IFS) meteorological product outside the U.S. For ground elevation, for the EMIT satellite instrument, we query values provided by that data source. For Tanager, we query the USGS GTOP030 Global Digital Elevation Map. For these dynamically queried or calculated parameters, we query a lookup-table database of unit absorption spectra that were precompiled and interpolated via MODTRAN simulations of various solar zenith angles, water vapor concentration, CH_4/CO_2 background concentration, and surface heights (Foote *et al.* 2021).

Plume Detection

A point source is defined as the geographic location from which emissions originate that results in a highly concentrated plume of CH_4 or CO_2 gas in the atmosphere. Plumes are an excess mass of concentration in the atmosphere produced by a specific source. Plumes from point sources are a subset of a broader class of CH_4 or CO_2 enhancements that may occur anywhere in the atmosphere as a result of point source and/or diffuse area sources that may or may not be co-located with the enhancements (e.g., a "cloud" of enhanced CH_4 can appear in the atmosphere some distance downwind of the actual source). This is a critical concept: *not all observed atmospheric enhancements are the result of a point source emission nor can those enhancements be reliably attributed to a specific emission source.* Therefore, Carbon Mapper point source detection and quality control procedures require that any detected atmospheric plume must be related to a credible point source on the earth's surface before reporting. Any observed enhancements that fail to meet quality control (QC) checks are noted for potential follow-up study but do not result in published plumes or emission rate estimates.

The Carbon Mapper point source detection process relies on concentration retrievals (CH_4 and CO_2 band images), visible red-green-blue (RGB) imagery from various observing systems, GIS data sets, and meteorological data. The process begins with automated application of CH_4 and CO_2 retrieval algorithms to every calibrated radiance strip image generated by a satellite or airborne sensor. This results in grayscale CH_4 and CO_2 band images that first undergo strip image level Quality Control (QC) review by human analysts. This review includes determination of systematic issues affecting the entire strip image, including retrieval processing problems, atmospheric artifacts (high haze,

https://doi.org/10.5194/egusphere-2025-2275
Preprint. Discussion started: 2 June 2025

clouds, smoke, etc), geolocation issues, or excessive noise. Each image's CH_4 and CO_2 band images are then reviewed to detect potential point source plumes along with geolocation of their likely origins.

790 2.5.3 Level 3-4 processing

Plume Segmentation

Following detection, Carbon Mapper implements an automated plume segmentation and delineation process on 795 identified and geolocated plumes. This process separates the background from enhanced CH_4/CO_2 pixels to create a masked plume boundary that is used for mass and emission quantification. The segmentation algorithm proceeds as follows (visual example in Fig. 10):

1. The L2B concentration map is cropped around the origin of a plume: ±2500 meters in both directions
800 2. A concentration threshold is dynamically determined to separate lingering background enhancements from plume enhancements. This threshold is subtracted off the cropped concentration map around the plume origin.
3. Connected pixels of enhanced concentration (> ppm-m threshold) are grouped together. A cluster must contain 5 pixels to be considered part of the plume.
4. A proximity metric is enforced on each cluster group. Separated clusters that exceed 15 pixels from the plume 805 origin are excluded from the plume

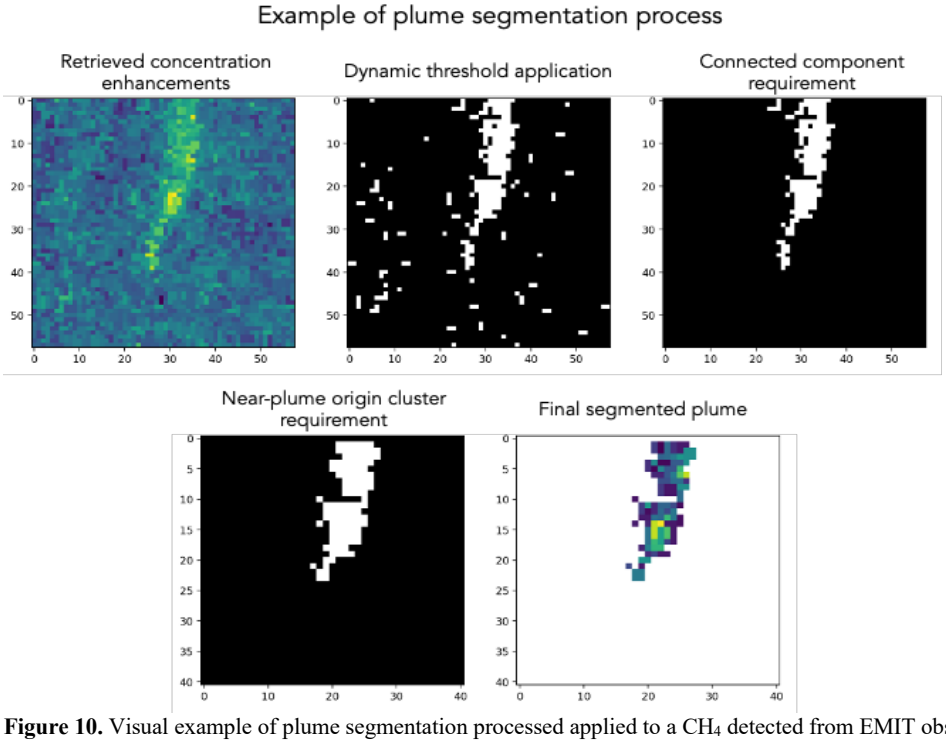

Figure 10. Visual example of plume segmentation processed applied to a CH_4 detected from EMIT observation.

810

Plume Emissions Quantification

For emissions quantification, we apply the Integrated Mass Enhancement (IME) approach, which calculates the excess mass in units of kilograms emitted to the atmosphere from a source (Thompson *et al.* 2016):

815 $$IME = \alpha \sum_{i=1}^{P} \Omega_i A_i \quad (5)$$

https://doi.org/10.5194/egusphere-2025-2275
Preprint. Discussion started: 2 June 2025

Where *i* refers to a single plume pixel, *P* is the number of pixels in the segmented plume mask, Ω is the concentration enhancement of that pixel, α is a unit conversion scalar (from ppm-m to kg/m^2), and A is the area of that pixel (m^2). We calculate an emission rate Q using the following relationship (Duren *et al.* 2019):

$$Q = \frac{IME}{L} U \quad (6)$$

Where U is the 10-m wind speed (m/s) and L is the plume length (m). Here U is taken from the HRRR 3km, 60 minute reanalysis product for observations within the U.S. and the ECMWFIFS 9 km product outside the U.S. Forecast versions of these products may be used for initial quick-look processing given standard latencies in receiving reanalysis products. In Equation 6, *L* is estimated as the maximum distance along the segmented plume's convex hull. For plumes covering large spatial distances, we impose a distance constraint such that the segmented plume mask is clipped to not exceed a 2500 m radial extent from the origin of the plume. Therefore, $L = \min\{\max(\text{hulldist}), 2500\text{m}\}$. The IME (Equation 5) is also only calculated within this clipped plume mask. This clipping procedure is employed to reduce bias that may affect IME quantification due to differing surface and meteorological conditions across large plumes, intermittency of the emission rate of the source, and to limit potential merging of multiple plumes downwind of their sources.

Quick look products

Carbon Mapper's workflow generates quick-look data products with a mean latency of < 36 hours following each observation. The quick-look product generation process includes a round of initial QC review by human analysts that generates quality flags for each plume that includes but are not limited to:

Strip image-level quality attributes

- Image artifacts [column, glint, flare, contrast, other]
- Low signal-to-noise flag
- Atmospheric artifacts [clouds, smoke, haze, other]
- Cloud cover fraction [0, 25, 50, 75, 100] or [0-1]

Plume-level quality attributes

- Overall rating (Good, Questionable, or Bad)
- plume shape flag
- artifacts intersect plume flag
- flare flag
- high background enhancement flag

Final Processing and Publication

Following generation of quick-look products, Level 4 processing proceeds with additional QC review of the initial emission estimate and additional processing including the use of reanalysis products in place of forecast wind fields. In some cases where there is high confidence in a plume detection but there are concerns with the fidelity of the emission estimate, Carbon Mapper will publish the plume image and coordinates but without an emission estimate. In addition to delivering final version of plume-level images, emission estimates, uncertainties and sector attribution, Level 4 processing includes aggregating a time-series of plumes to a specific emission source on the earth's surface and calculating persistence-adjusted average emission rates for that source following methods described in Cusworth *et al.,* 2021a. The resulting plume raster images and tabular information on emission rates, plume/source coordinates, sector attribution, detection dates/times, source persistences, and associated uncertainties as well as our Level 2 strip-image level products are published via Carbon Mapper's public data portal and available for API and bulk download 30 days following each Tanager observation. Additional Carbon Mapper documentation including our Data Product Guide, Algorithm Theoretical Basis Documents, and Quality Control Description Document are available in the Technical Resources section of our website (https://carbonmapper.org/resources/technical-resources).

https://doi.org/10.5194/egusphere-2025-2275
Preprint. Discussion started: 2 June 2025

3 Tanager-1 commissioning: demonstration of key capabilities

Here we present an initial demonstration of key system capabilities using observations acquired during the first seven months of Tanager-1 operations following instrument activation. After a month of spacecraft and instrument initialization and checkout, a First Light Campaign was conducted between September and December 2024. During this time the satellite orbit was gradually lowered from an average altitude of about 510 km to 430 km – resulting in an instrument FOV and spatial resolution that was initially 6-26% larger than that planned for the final operational orbit. The temporally coarser spatial resolution translated to CH_4 and CO_2 detection limits somewhat higher than expected for nominal operations. During the First Light Campaign, imaging was limited to about 1 observation per orbit on average, most observations were conducted in the Standard (lowest) sensitivity imaging mode, and the length of each image was significantly shorter than available in nominal operations. Despite these limitations, this provided an opportunity to exercise the critical satellite subsystems and enabled a preliminary assessment of the end-to-end performance of the Carbon Mapper emissions monitoring system. Starting in January 2025, Tanager-1 began a multi-month transition to steady state operations, with a steady ramp-up in image size and number of daily observations as well as increased use of Maximum sensitivity imaging mode. This paper includes some early results from this transition phase.

Figure 11 shows a first-light hyperspectral data cube from a Tanager-1 observation of Karachi, Pakistan acquired on September 16, 2024, one month after launch. The first CH_4 plume detected by Tanager-1 in that image was attributed to a known waste dump. The estimated emission rate is 1631 ± 326 kgCH_4/h. The plume was detected and quantified within 12 hours of the observation. Subsequent analysis of over 1400 plumes detected between Feb 1 and April 1, 2025 indicate good performance against our 72 hour data latency requirement: median 10 hours, mean 34 hours between Tanager image acquisition and Carbon Mapper plume detection. As an illustration of Tanager's broader hyperspectral imaging utility including CH_4, CO_2 and multiple other environmental variables, Fig. 12 plots the Top Of Atmosphere (TOA) reflectance across the full VSWIR spectral range for 3 pixels in the Karachi image.

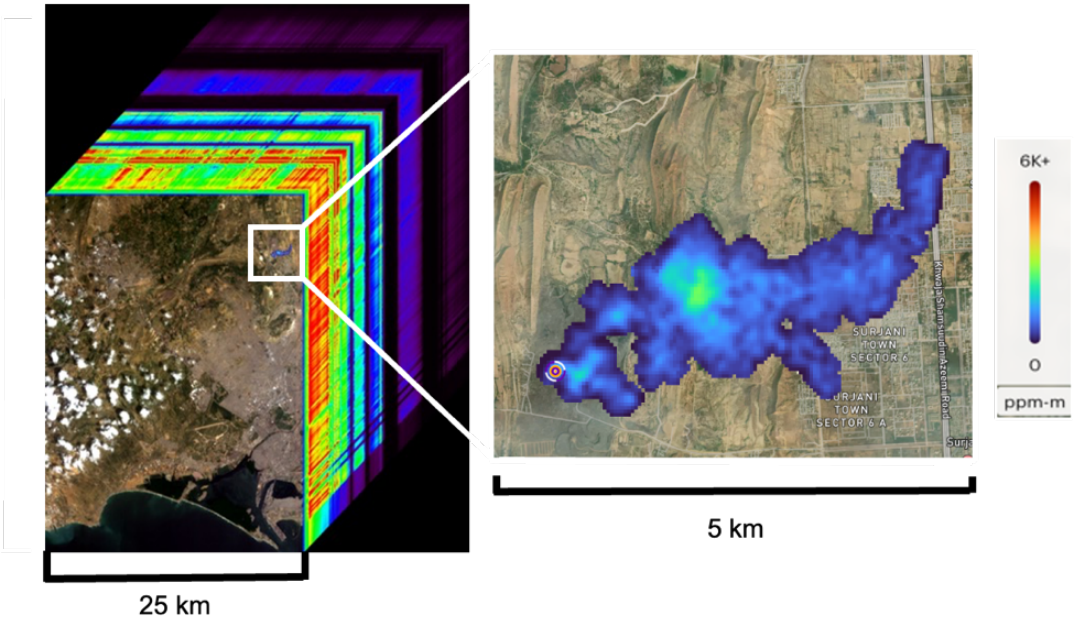

Figure 11. (Left) Hyperspectral data cube from Tanager-1 first light observation of Karachi, Pakistan on September 16, 2024, one month after launch. (Right) The first CH_4 plume detected by Tanager-1 at a waste dump within the same image, overlaid on a non-contemporaneous Planet high resolution Skysat visible image. The estimated emission rate is 1600 ± 300 kgCH_4/h. The plume was detected and quantified within 12 hours of the observation.

https://doi.org/10.5194/egusphere-2025-2275
Preprint. Discussion started: 2 June 2025

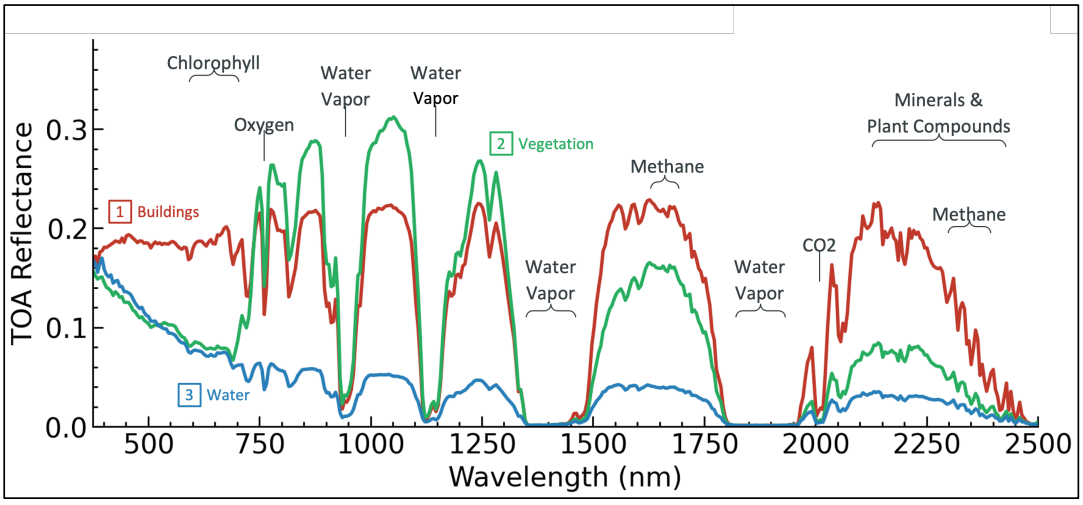

Figure 12. Plots of full VSWIR Top Of Atmosphere (TOA) reflectance from 3 pixels containing buildings [1], vegetation [2], and water [3] in the image in Figure 11 illustrating Tanager's hyperspectral sensitivity to CH_4, CO_2, and multiple other environmental variables.

Between September 16, 2024 and April 15, 2025, Tanager-1 completed about 5200 observations distributed globally (Fig. 13, top panel), about one-third of which were over known high emission regions. During this period, we detected 2483 CH_4 and 460 CO_2 point source emission plumes (Fig. 13, bottom panel). Until January 2025 most images were collected in Standard (1x8) Sensitivity imaging mode with shorter than normal line lengths (e.g., <= 100 km) and at initial higher orbital altitudes ranging from 430 to 510 km. Tanager-1 only began imaging Carbon Mapper's priority tasking deck in February 2025 as we prepared to transition to fully operational data collection. Roughly two-thirds of Tanager-1 observations through April 15, 2025 were repeated observations of diverse land or ocean calibration sites or island chains in support of non-trace gas hyperspectral applications where one would not expect to see strong CH_4 or CO_2 emissions.

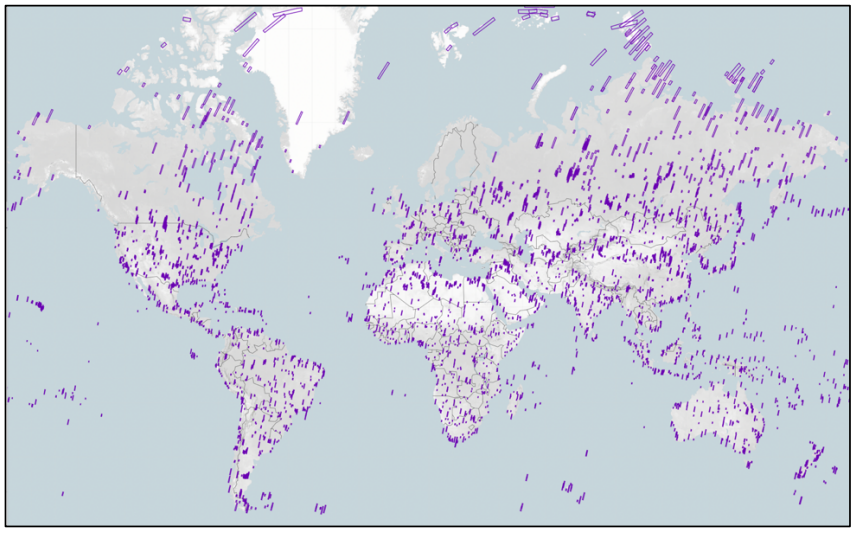

https://doi.org/10.5194/egusphere-2025-2275
Preprint. Discussion started: 2 June 2025

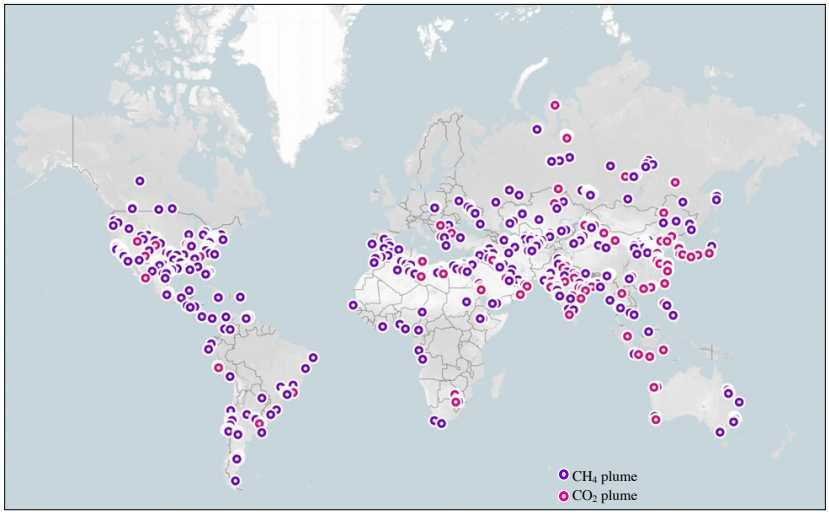

Figure 13. Map of about 5200 Tanager-1 strip image outlines (top) and about 2900 CH_4 and CO_2 plume detections (bottom) for the first seven months of operation following instrument activation (September 16, 2024 – April 15, 2025).

One motivation for Tanager high spatial resolution mapping is to help address the lack of granular CH_4 and CO_2 data in the tropics and other persistently cloudy regions that otherwise can remain unobserved for months or years. Frankenberg *et al.* (2024) analyzed global observations by the Sentinel-2 satellite with 10 meter spatial resolution and 5 minute mean revisit interval to show that satellites with a 30 meter spatial resolution and wide area mapping should achieve median cloud-free (< 0.1% of a pixel) coverage in the Amazon of 10% and 20% during the rainy and dry season, respectively. In contrast, satellites with 1 km spatial resolution would achieve cloud-free yields of only 0.5% and 2% for the wet and dry seasons and satellites with > 2 km spatial resolution would achieve < 0.1% cloud free yields. For reference, the current premier global CH_4 flux mapping satellite (Sentinel-5p/TROPOMI) has a nadir spatial resolution of about 7 km. To evaluate Tanager performance in tackling cloudy images, we targeted several oil and gas basins, landfills and coal mines in the tropics. Figure 14 shows an example of a cloudy image acquired by Tanager-1 in February 2025 in Venezuela (panel A). Carbon Mapper detected a CH_4 plume from an oil and gas facility with roughly 120 meters separation from the nearest cloud (panel B). A PlanetScope 5 meter resolution visible image of the same area the same month with no clouds clearly shows the oil and gas facility (panel C). Tanager-1 has successfully detected similar plumes at multiple sites across the tropics, demonstrating the promise of sustained high-resolution mapping of these critical regions.

Another major design driver for the Tanager instrument is to be robust to challenging observational scenarios including high latitude regions such Russia and Canada where low sun elevation angles and low SWIR albedos from snow covered surfaces can impact SNR and degrade CH_4 and CO_2 detection limits. To evaluate Tanager-1 performance in these conditions we conducted observations of representative high latitude oil and gas production regions during the northern hemisphere winter. Figure 15 shows the results of two such images in Russia in February at 55 degN and 66 deg N latitude. In each case, the ground is covered in snow and solar zenith angles exceeded 70 degrees, however Tanager-1 detected multiple CH_4 plumes. For reference, Kayrros analysis (Kayrros 2025) of Sentinel-5p/TROPOMI observations between Jan 2019 and March 2025 reported 482 CH_4 point sources at latitudes higher than 50 degN ranging from 2800 to 394,000 kgCH_4/h (mean 50,000 kgCH_4/h). As of early April 2025, Kayrros did not report TROPOMI detections for any of the Tanager-1 CH_4 plumes shown in Fig. 15.

https://doi.org/10.5194/egusphere-2025-2275
Preprint. Discussion started: 2 June 2025

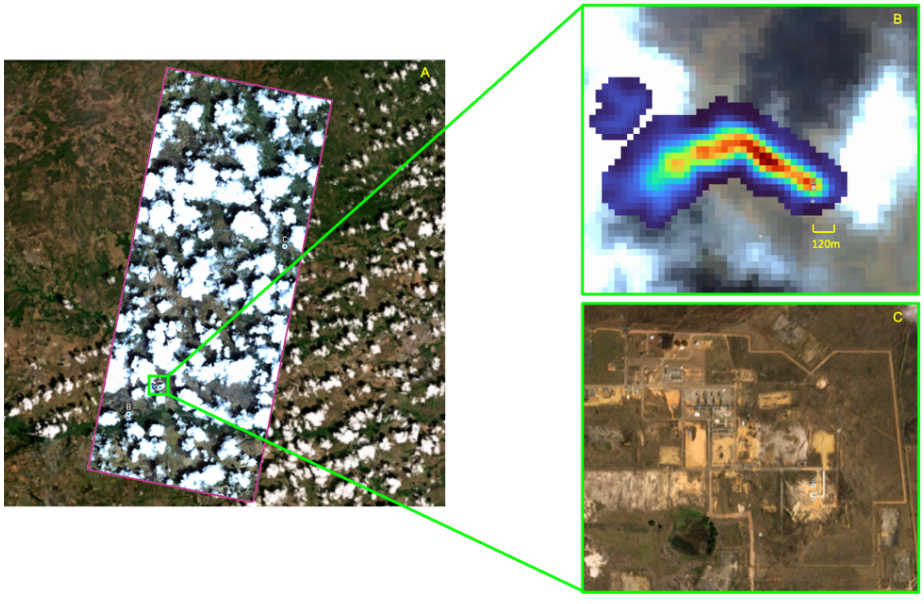

Figure 14. Tanager-1's 30 meter spatial resolution enables detection of CH_4 plumes in perpetually cloudy regions such as the tropics. In this example of a cloudy image of Venezuela (panel A), Carbon Mapper detected a CH_4 plume from an oil and gas facility with a roughly 120 meters separation from the nearest cloud (panel B). A PlanetScope 5 meter resolution visible image of the same area in February 2025 with no clouds clearly shows the oil and gas facility (panel C). The basemap overlaid by the Tanager image on the left is ©Mapbox, ©OpenStreetMap, and ©Maxar.

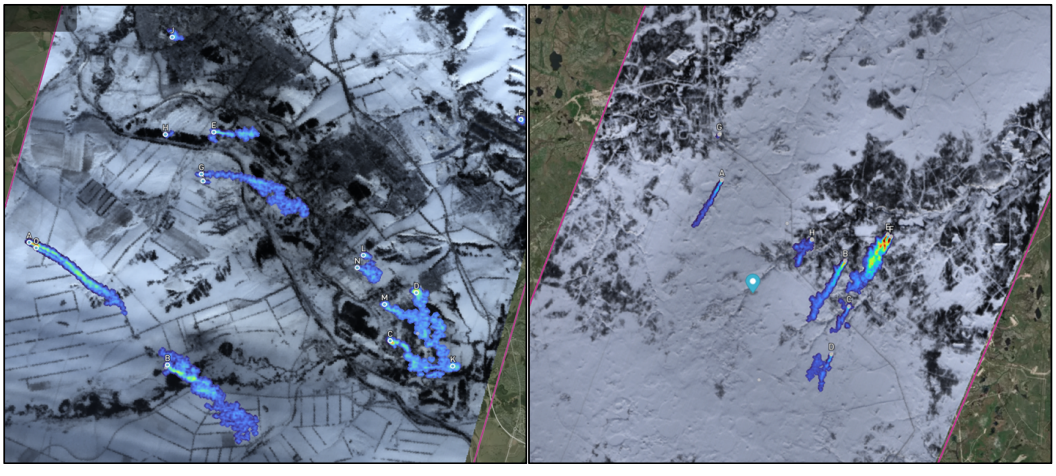

Figure 15. Two examples of Tanager's CH_4 detection capabilities for challenging high latitude winter images in Russia due to large solar zenith angles and low SWIR albedo due to snow covered surfaces. (left) 20 x 20 km^2 subset of a Tanager-1 image at 55 deg N latitude with 13 CH_4 plumes detected on Feb 23, 2025 at 05:51:06 UTC. Emission estimates for the plumes in this image range from about 400 to 2500 $kgCH_4/h$. (right) 24 x 24 km^2 subset of a Tanager-1 image at 66 deg N latitude with 6 CH_4 plumes detected on Feb 26, 2025 at 06:54:41 UTC. Emission estimates for plumes in this image range from about 670 to 5000 $kgCH_4/h$. The basemap overlaid by the Tanager image in each case is ©Mapbox, ©OpenStreetMap, and ©Maxar.

https://doi.org/10.5194/egusphere-2025-2275
Preprint. Discussion started: 2 June 2025

As described in section 2.4, Tanager is also designed to detect CH_4 emissions over ocean surfaces which are dark at SWIR wavelengths. To evaluate Tanager glint-mode performance we conducted several multiple sun-glint observations of selected offshore oil and gas production basins. Figure 16 shows a Tanager-1 detection of a CH_4 plume from an oil and gas platform in the Moho Nord block off the coast of the Republic of the Condo. We intend to scale up glint-mode observations of other offshore production areas within the first year of Tanager-1 operations.

Another key objective of Carbon Mapper's observing strategy is to routinely monitor high emission point sources to assess their variability and persistence. During the first 6 months of Tanager-1 operations following instrument activation and checkout, we were able to track some emitters with a regular sample cadence. Figure 17 shows one such example: a time-series of CH_4 plumes detected by Tanger-1 at a persistently emitting oil and gas production site in Algeria. Tanager-1 observations occurred on a roughly monthly basis on average from October 2024 through April 2025.

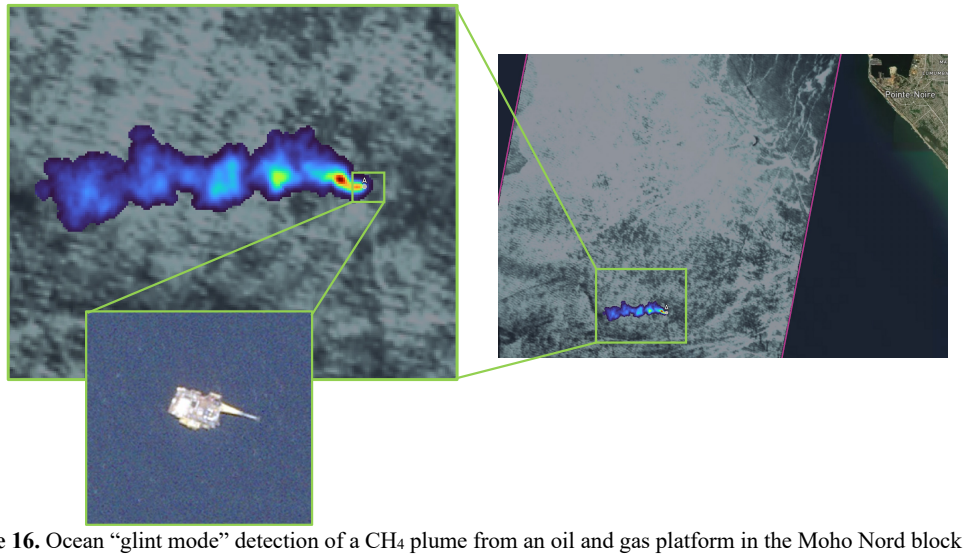

Figure 16. Ocean "glint mode" detection of a CH_4 plume from an oil and gas platform in the Moho Nord block 20 km off the coast of the Republic of the Congo. CH_4 image derived from a Tanager-1 observation on March 10, 2025 at 10:19:13 UTC. The estimated emission rate is 2322 ± 254 kgCH_4/h. The basemap in the inset zoom view is from a Planet SkySat visible image (70 cm resolution) acquired March 16, 2025, providing clear attribution of the likely source origin. The basemap overlaid by the Tanager image in the right figure is ©Mapbox. ©OpenStreetMap, and ©Maxar.

To evaluate Tanager's ability to detect CH_4 and CO_2 point sources simultaneously, we observed some of the world's larger cities and industrial regions that host fossil energy production, electricity generation and refineries. This resulted in numerous individual images where multiple CH_4 and CO_2 plumes were detected. Figure 18 is one such example. Tanager-1 imaged Bahrain on April 1, 2025, revealing 8 CH_4 plumes from oil and gas operations and 2 CO_2 plumes from gas fired power plants. The distribution of plume sizes and shapes reveals both the diversity of emission rates and surface wind fields that are common to many regions.

https://doi.org/10.5194/egusphere-2025-2275
Preprint. Discussion started: 2 June 2025

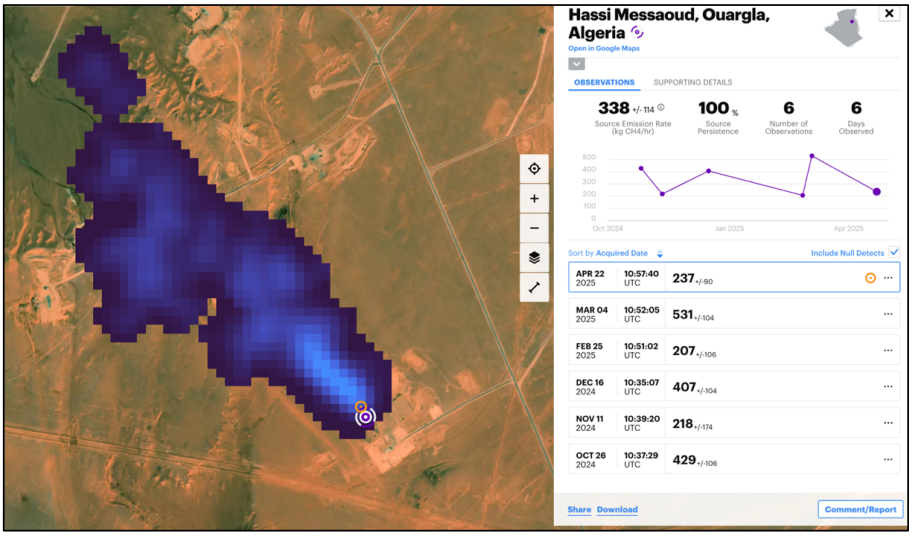

Figure 17. Screenshot from Carbon Mapper's public data portal showing a time series of CH_4 plumes detected by Tanger-1 at a persistently emitting oil and gas production site in Algeria. Tanager-1 observations occurred on monthly cadence on average from October 2024 through April 2025. . Basemap image ©Mapbox, ©OpenStreetMap, and ©Maxar.

Tanager-1 commissioning also provided an opportunity to conduct some leak detection and repair pilot efforts that build on our previous experience with aircraft prototyping. Figure 19 shows a methane plume from a leaking oil and gas gathering pipeline that was detected in the Texas Permian basin from a Tanager-1 observation on Oct. 9, 2024 with an estimated instantaneous emission rate of 7100 ± 1100 kgCH_4/h. After Carbon Mapper notified federal and state agencies the next day, the leak was reported to be voluntarily fixed by the operator. A subsequent Tanager observation on Oct. 24 detected no methane at that location. This early demonstration bodes well for Carbon Mapper plans to scale-up data sharing with facility operators and expanded mitigation progress globally.

4 Performance predictions and validation

In addition to the various functional demonstrations during Tanager-1 commissioning, a series of experiments were conducted to provide quantitative validation of key performance parameters. Maximum CH_4 and CO_2 performance should occur when Tanager-1 reaches its final target altitude (406 km) and LTDN (1200 hours). Additionally, instrument and detection performance is best assessed by completing a statistically robust number of blinded controlled release experiments sufficient to determine probabilistic detection limits. However, these initial experiments of on-orbit measurements provide strong empirical grounding in our predicted ultimate performance.

4.1 Single measurement precision and detection limits

The Minimum Detection Limit (MDL) for CH_4 point sources as a function of measurement precision can be estimated using the method described by Jacob *et al* 2016 as follows:

$$MDL = 2\frac{M_{CH4}}{M_a}\frac{UWp\sigma}{g} \quad (7)$$

Where M_a = 0.029 kg/mol and M_{CH4} = 0.016 kg/mol are the molecular weights of dry air and methane, p is the dry atmospheric surface pressure (typically about 1000 hPa), and g = 9.8 m/s^2 is the acceleration of gravity, U is the wind speed in m/s, W is the pixel size in meters. σ is the single measurement precision or the ability to detect a localized enhancement of CH_4 relative to the average local background (assumed here to be 1800 ppb). A similar approach can be used to estimate the MDL for CO_2 point sources.

https://doi.org/10.5194/egusphere-2025-2275
Preprint. Discussion started: 2 June 2025

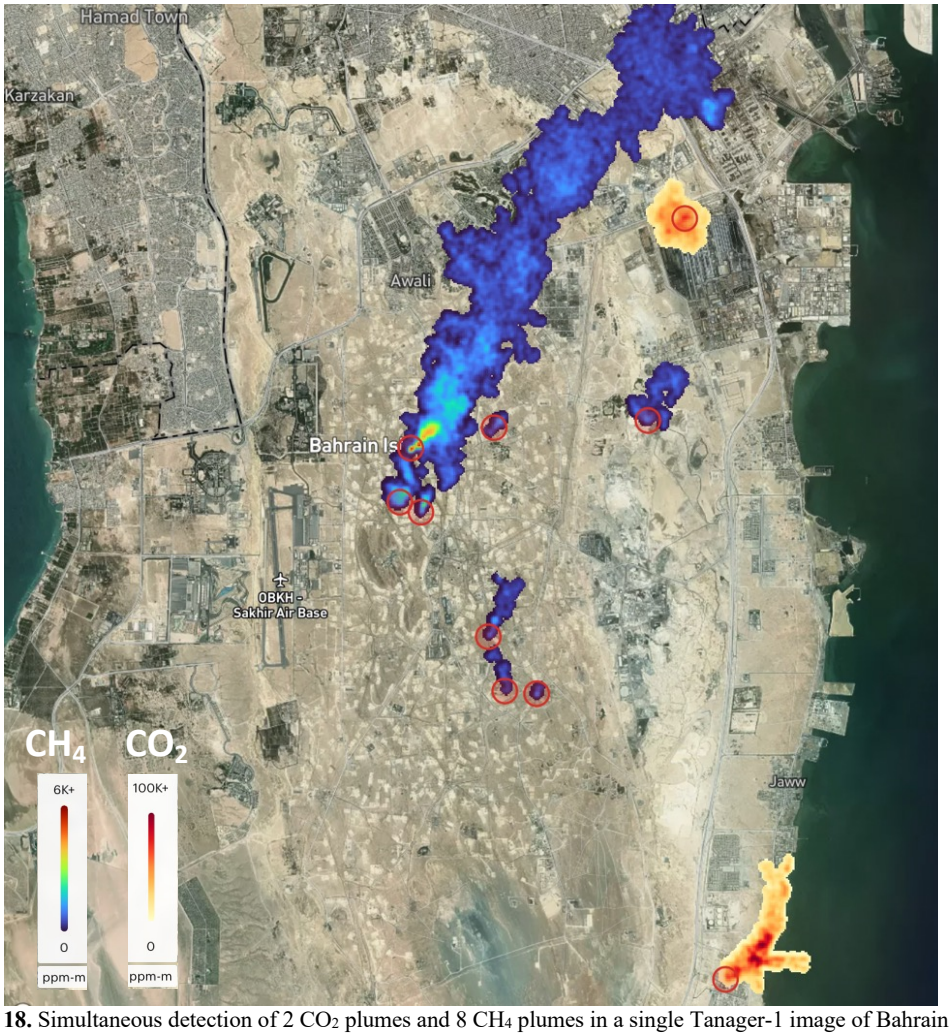

Figure 18. Simultaneous detection of 2 CO_2 plumes and 8 CH_4 plumes in a single Tanager-1 image of Bahrain acquired on April, 2025. The CO_2 plumes are attributed to gas-fired power plants. The CH_4 plumes are attributed to oil and gas production. Basemap image ©Mapbox, ©OpenStreetMap, and ©Maxar.

https://doi.org/10.5194/egusphere-2025-2275
Preprint. Discussion started: 2 June 2025

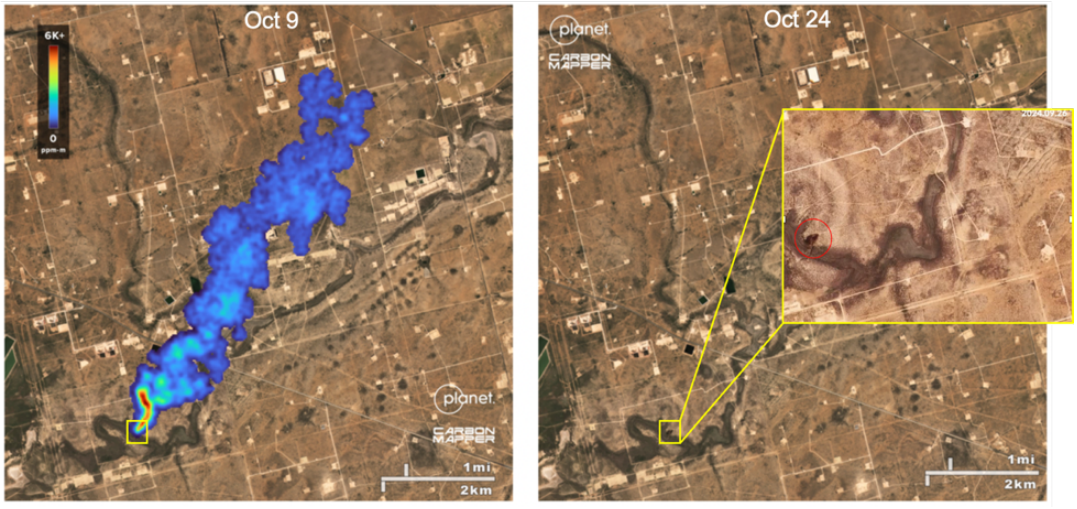

Figure 19. (Left) a large methane plume from a leaking oil and gas gathering pipeline was detected in the Texas Permian basin from a Tanager-1 observation on Oct. 9, 2024 with an estimated instantaneous emission rate of 7100 ± 1100 kgCH_4/h. Carbon Mapper notified federal and state agencies the next day who informed the operator who reported that the leak was promptly repaired. (Right) a subsequent Tanager observation on Oct. 24 detected no methane. The inset image on the right from Planetscope visible band observations indicated a sudden darkening of the surface within 30 meters of the origin of the methane plume shortly before the first Tanager-1 observation, consistent with a potential condensate release from the pipeline. . Basemap image ©Mapbox, ©OpenStreetMap, and © Maxar.

Instrument spectral performance (sampling and FWHM) and radiometric performance (SNR) are the primary constraints on σ. For Tanager, spectral sampling (5nm) and FWHM (approaching 5nm in the SWIR bands) were set by instrument design and alignment as described in section 2. SNR is a more complex function of the instrument design (optical throughput, read noise, etc) and operation (effective integration time) as well as environmental factors such as solar zenith angle, surface albedo and various atmospheric variables. Prior to Tanager-1 launch we used the lab-measured instrument spectral (Fig. 3) and radiometric (Fig. 4) performance to generate theoretical predictions of the single measurement CH_4 precisions for each imaging mode (Table 4). We simulated a top-of-the atmosphere radiance spectrum for 35 degree solar zenith angle, 25% albedo using the MODTRAN6 radiative transfer model, and then applied the measured Tanager instrument noise. We applied the optimal estimation concentration retrieval algorithm IMAP-DOAS (Frankenberg *et al.* 2005), which provides single-sounding posterior precision for a retrieved column-averaged CH_4 or CO_2 column concentration. We then applied equation 7 and an assumed wind speed of 3 m/s and 30 meter pixel size to calculate the predicted CH_4 MDL for each imaging mode (Table 4).

However, a more direct measure of σ with the as-built system can be obtained empirically by plotting the standard deviation of background CH_4 in units milli-moles/m^2 across over full image strips as a function of surface albedo for over 300 Tanager observations spanning a wide range of solar zenith angles. Figure 20 provides a preliminary empirical assessment derived from Maximum and Standard sensitivity observations where σ is calculated as the standard deviation of non-plume background CH_4 within an image strip using the Columnwise Matched Filter algorithm that is the core of Carbon Mapper's operational data workflow. Figure 21 provides a histogram of the distribution of precisions for a subset of those images with albedos ranging from 0.2 to 0.3 (average 0.25) and solar zenith angle (SZA) ranging from 40 to 50 degrees (average 45 degrees). The resulting mean σ for these images is 6.32 mmol/m^2, (0.97%, assuming 650 mmol/m^2 background) and 13.77 mmol/m^2 (2.12%) for Maximum and Standard sensitivity imaging modes, respectively. Those values are equivalent to a CH_4 MDL of 66 and 140 kgCH_4/h, respectively, for a 30 meter pixel size and 3 m/s wind speed (Table 5). This is in good agreement with pre-launch predictions, particularly considering that the former used the higher sensitivity IMAP-DOAS algorithm.

https://doi.org/10.5194/egusphere-2025-2275
Preprint. Discussion started: 2 June 2025

Repeating this exercise for CO_2 and assuming 109,030 mmol/m^2 backgrounds we estimate single measurement precisions of 0.30% and 0.52% and MDL of 10,500 and 19,600 kgCO_2/h, respectively, for Maximum and Standard sensitivity modes. As discussed in section 2, our MDL requirements were derived from an ultimate goal of a 90% POD of 100 kg/CH_4 which should be achievable with the as-built Tanager precision and spatial resolution however completion of additional empirical field testing will be necessary for confirmation.

Table 4. Pre-launch predictions of single measurement precision and MDL for CH_4 point sources by imaging mode using measured instrument performance and modeled radiances for plumes assuming 25% albedo, 35 degree solar zenith angle, 3 m/s wind speed and 406 km orbit altitude. Additionally, a prediction of CH_4 90% Probability of Detection (POD) is derived from a linear relationship between MDL and POD observed in empirical field testing of similar airborne instruments.

Imaging Mode (Sensitivity)	CH_4 single measurement precision (%)	CH_4 MDL (kg/h)	CH_4 90% POD (kg/h)
Maximum	0.94 %	63	90
High	1.07 %	73	100
Medium	1.35 %	92	125
Standard	1.99 %	135	180

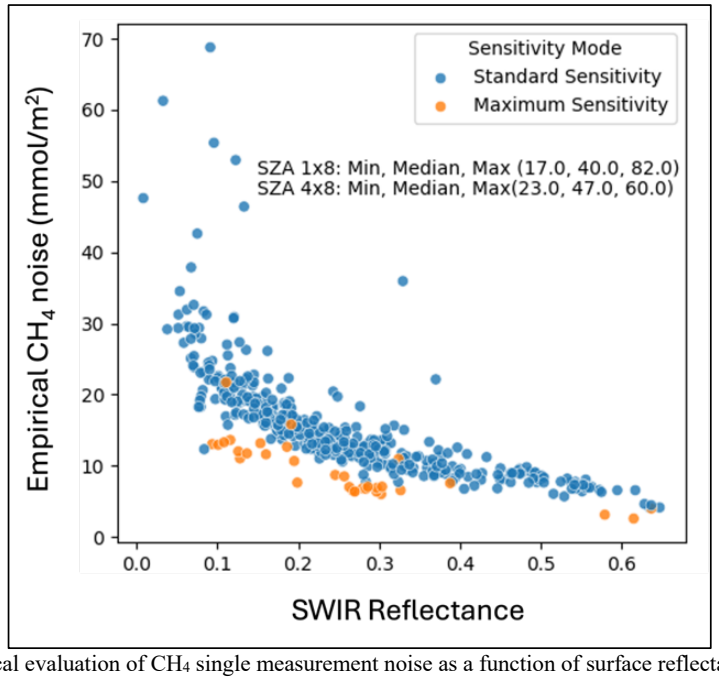

Figure 20. Empirical evaluation of CH_4 single measurement noise as a function of surface reflectance for different imaging modes during Tanager-1commissioning.

https://doi.org/10.5194/egusphere-2025-2275
Preprint. Discussion started: 2 June 2025

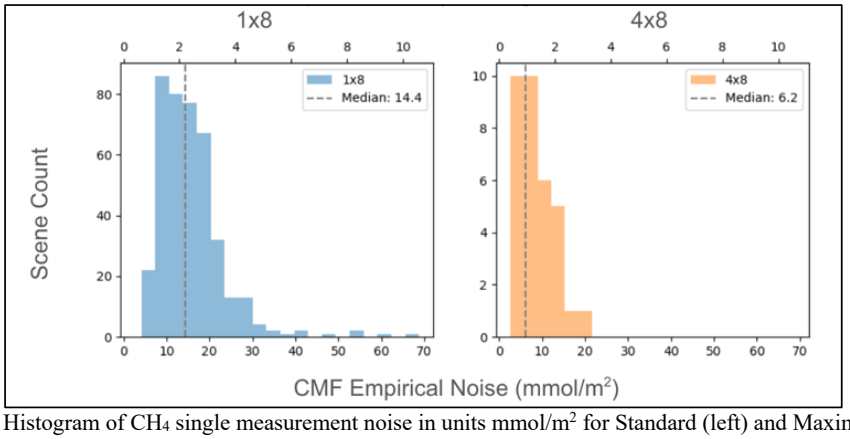

Figure 21. Histogram of CH_4 single measurement noise in units mmol/m^2 for Standard (left) and Maximum (right) sensitivity imaging modes during Tanager-1 commissioning. The colored band indicates the interquartile range.

Table 5. Single measurement CH_4 precision and MDL for Maximum and Standard imaging modes derived from Tanager on-orbit observations. Empirical precision is calculated from the standard deviation of background CH_4 (assuming 650 mmol/m^2 background) and CO_2 (assuming 109,030 mmol/m^2 background) across entire images using the operational CMF retrieval algorithm. This calculation was performed on Tanager-1 images with albedos ranging from 20 to 30% (mean 25%) and solar zenith angles ranging from 40 to 50 degrees (mean 45 degrees). This empirical assessment is more conservative than the theoretical pre-launch predictions which used the higher precision IMAP-DOAS algorithm on a simulated image with a smaller solar zenith angle.

Imaging Mode (Sensitivity)	**Mean CH_4 Measurement Precision**	**CH_4 MDL (kg/h)**	**Mean CO_2 Measurement Precision**	**CO2 MDL (kg/h)**
Maximum (4x8)	0.97%	66	0.30%	10,400
Standard (1x8)	2.12%	144	0.52%	19,600

4.2 Validation against independent measurements

Empirical studies (e.g., Sherwin *et al.* 2024, Ayasse *et a.l* 2023) underscore the importance of looking beyond simple analytic predictions of MDL to specify a 90% POD that reflects real world performance over a broader range of conditions. The latter requires a statistically robust set of blinded controlled release tests (e.g., typically > 50 samples which for most satellites can require up to a year to complete when limited to a single test site). While single-blind controlled release testing of Tanager-1 is underway now and anticipated to continue through 2025, we have conducted some initial experiments in the meantime that provide confidence in our pre-launch performance predictions.

During Tanager-1 commissioning phase JPL's AVIRIS-3 aircraft instrument (Green *et al.,* 2022) conducted coordinated under-flights over known high CH_4 emitting regions across the western US, typically at 9 km altitude. The objective of these flights was to provide contemporaneous observations of the same CH_4 sources observed by Tanager-1 including super emitters in oil and gas basins across New Mexico and California. Figure 22 shows good agreement for 20 CH_4 plumes detected by contemporaneous (mean temporal separation < 15 minutes) mapping by AVIRIS-3 and Tanager-1 of the Permian Basin. Additionally, Tanager-1 participated in some cooperative (unblinded) controlled release tests at sites in Wyoming and Arizona designed and operated by a Stanford/University of Michigan research team. That team has established a capability to provide independent evaluation of methane

https://doi.org/10.5194/egusphere-2025-2275
Preprint. Discussion started: 2 June 2025

detection limits and emission estimates from satellites, including a single-blind test program for multiple satellites that began operations in January in 2025.

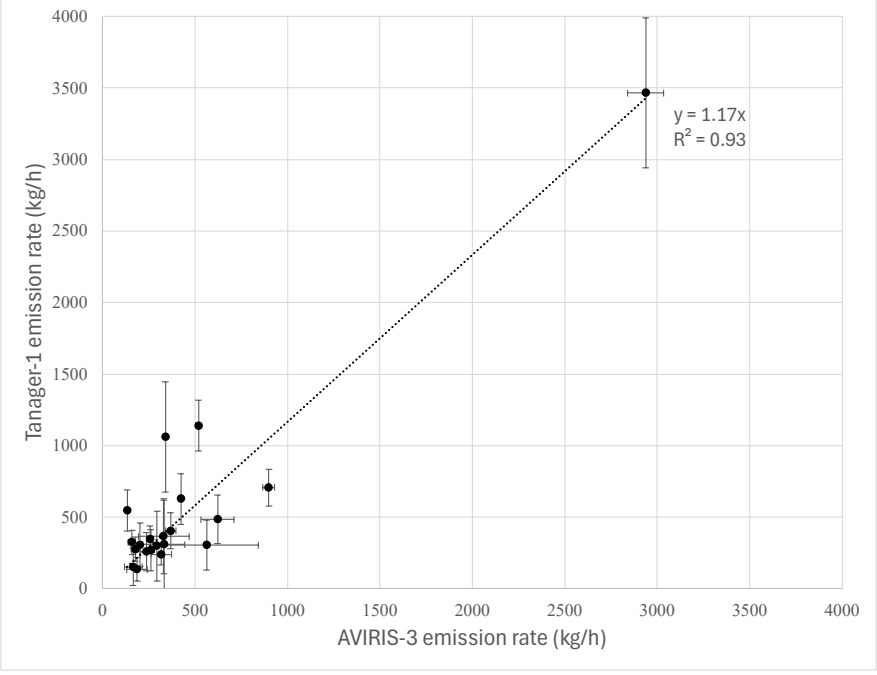

Figure 22. Comparison of Carbon Mapper emission estimates for 20 CH_4 plumes observed by both AVIRIS-3 and Tanager-1 during near-simultaneous overpasses. The median separation between observations was 12 minutes (mean 15 minutes, maximum 37 minutes). The slope and R^2 for an ordinary least squares fit are shown. The error bars represent 1 standard deviation uncertainties in the Tanager-1 and AVIRIS-3 emission rate estimates.

Unblinded controlled release experiments of were conducted between September 21 and October 16, 2024, in Evanston, Wyoming (41.275815, -110.930561), and between November 4 and December 31, 2024, in Casa Grande, Arizona (32.821921, -111.785396). Natural gas was released from a system consisting of a compressed natural gas trailer connected to a pressure regulation trailer and a gas metering trailer. Flow rates were metered using one of three parallel-mounted Emerson Micromotion Coriolis flow meters, directing gas through a 7.3 m stack controlled by a butterfly valve (El Abbadi *et al.,* 2024). The flow rate was controlled virtually via a flow control system on the metering trailer. Meteorological data were collected near the release point at 10 m (Campbell Scientific CAST3B, 3D) and 2 m (Campbell Scientific METSENS500, 2D) heights, providing measurements of wind speed and wind direction at 10 m and 2 m as well as relative humidity, dew point, temperature, and atmospheric pressure at 2 m. The test team also tracked natural gas composition, which ranged from 92.7% to 94.5% CH_4 throughout the unblinded period. In Evanston, six unblinded releases were conducted, with emission rates ranging from 186.1 (± 3.5% 95% CI) to 694.2 (±3.59% 95% CI) kg/h. In Casa Grande, nine releases ranged from 98.85 (± 8.57% 95% CI) to 951.5 (± 5.34% 95% CI) kg/h. During the unblinded period, mean wind speeds in Evanston were 4.78 m/s within 30 minutes of noon and mean wind speeds in Casa Grande were 2.16 m/s within 30 minutes of noon. Release rates and meteorological observations were rapidly shared following Tanager satellite overpasses during this period, and can be found in this repository: https://doi.org/10.25740/qh001qt3946. The releases during this unblinded period were performed cooperatively, with flow rates and durations suggested by the Carbon Mapper team.

Uncertainties associated with this controlled release configuration are smaller than those associated with the quantification of gas flow rates from satellites. The accuracy of the metered gas flow rate as metered by Emerson

https://doi.org/10.5194/egusphere-2025-2275
Preprint. Discussion started: 2 June 2025

Micromotion coriolis flow meters ranged from ± 0.25% for the large (CMFS150M) and small (CMFS015H) meters, to ± 0.35% for the medium meter (CMF050M). Uncertainties associated with the meteorological measurements were also small. 10-m measurements from the CSAT3B has a maximum offset error in wind speed of ±8 cm/s (U_x, U_y) and ± 4 cm/s (U_z), and a maximum gain error of ±2%, 3%, or 6% depending on whether wind vector is within 5, 10, or 20 degrees of horizontal respectively. The 2-m measurements from the METSENS500 were accurate in wind speed to within 3% and wind direction to within 5 degrees up to 40 m/s, with those figures changing to 5% and 5 degrees for winds between 40 m/s and 60 m/s.

Figure 23 shows an example of near-simultaneous (< 30 second separation) observations of one such controlled release test on November 4, 2024 by AVIRIS-3 and Tanager-1. In addition to consistent visual plume appearance, Carbon Mapper's analysis of the Tanager-1 and AVIRIS-3 observations resulted emission estimate that agree to within about 10% and plume geolocation estimates that agree to within 20 meters. Figure 24 compares Carbon Mapper's estimated emission rates and the Stanford/U. Michigan reported emission rates for the 11 unblinded releases observed by Tanager-1. The slope and R^2 of an ordinary least squares fit is shown for those observations of the two release sites.The majority of the Tanager observations here were acquired using standard sensitivity (1x8) imaging mode and at initial higher orbital altitudes ranging from 430 to 510 km. Additionally, most of these tests occurred between November and December at the start of the northern hemisphere winter with lower sun elevations. These tests did not attempt to probe the Tanager detection limits given the system was not yet at peak sensitivity.

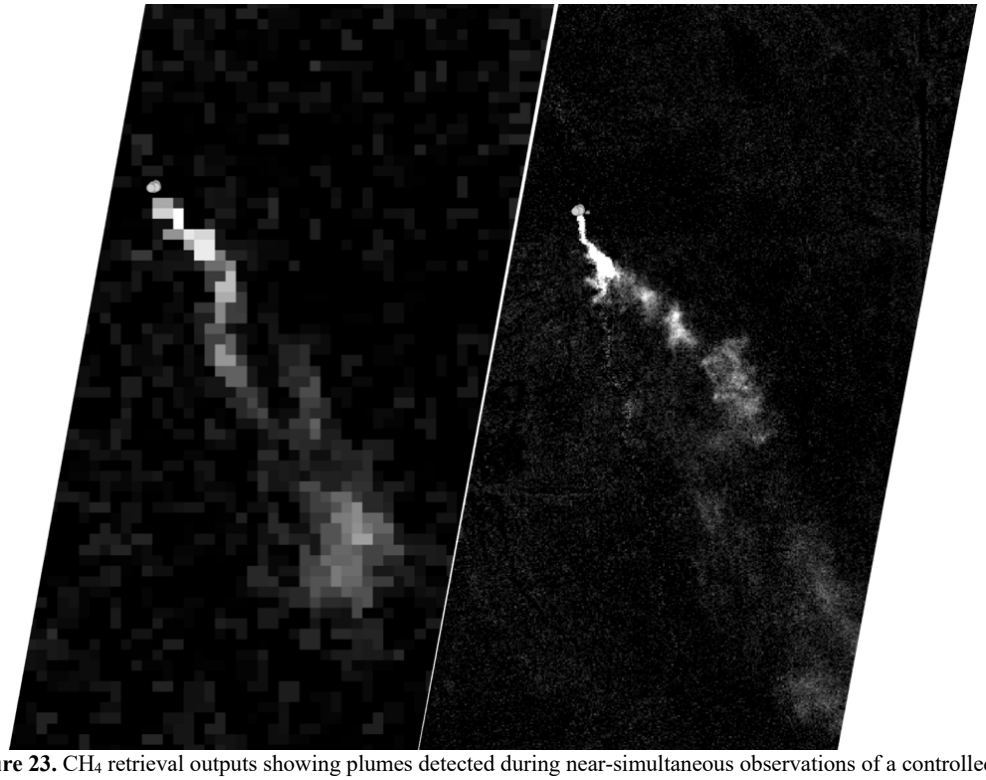

Figure 23. CH_4 retrieval outputs showing plumes detected during near-simultaneous observations of a controlled release test in Arizona on November 4, 2024 with Tanager-1 at an altitude of about 500 km at 18:16:42 UTC (left panel) and AVIRIS-3 at an altitude of 9 km at 18:17:10 UTC (right panel). The geolocation of the methane plume from the two observations agreed to within 20 meters. The emission rate estimate for the single Tanager-1 image was 775 ± 111 $kgCH_4/h$. The mean emission rate from three AVIRIS-3 observations within 10 minutes of the Tanager overpass was 882 ± 133 $kgCH_4/h$. The mean metered emission rate as reported by the controlled release team corresponding to the three AVIRIS-3 observations was 859 ± 49 $kgCH_4/h$.

https://doi.org/10.5194/egusphere-2025-2275
Preprint. Discussion started: 2 June 2025

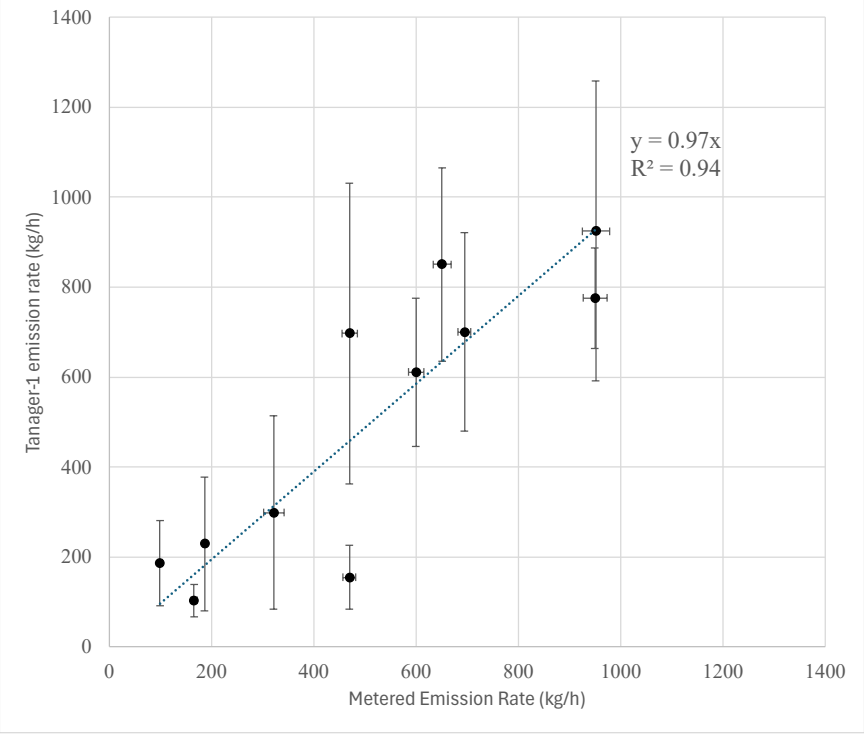

Figure 24. Comparison of Carbon Mapper estimated emission rates and metered emission rates from the Stanford/U. Michigan controlled release team for cooperative (non-blind) testing of Tanager-1 at test sites Arizona and Wyoming. The slope and R^2 for an ordinary least squares fit are shown. The error bars represent 1 standard deviation uncertainties in the Tanager-1 emission estimates and metered emission rates. Most of the observations shown here were using standard sensitivity (1x8) imaging mode and at initial higher orbital altitudes ranging from 430 to 510 km. These initial experiments were designed to provide an initial evaluation of precision and bias rather than probing detection limits and do not represent final sensitivity.

4.3 Spatial and temporal coverage

As described in section 2.1, Carbon Mapper's objective of optimizing Observing System Completeness requires maximizing spatial coverage and temporal sampling. This motivates the deployment of a constellation of satellites. For a given spatial tasking deck, temporal sampling is primarily set by the number of satellites, the satellite orbits, cross-track pointing agility, and instrument FOV. To address these factors, Fig. 25 plots the Median Time To Access (TTA) for an isolated of interest (AOI) as a function of latitude and number of satellites. This illustrates that the median TTA for a single Tanager satellite can range from about 2 to 8 days at mid-latitudes (30-40 deg) but with four satellites drops to ≤ 12 hours. Figure 26 shows the mean, maximum, and 90 percentile times to access for a constellation of four Tanager satellites which demonstrates that such a constellation is capable of sub-daily monitoring at high priority sites.

https://doi.org/10.5194/egusphere-2025-2275
Preprint. Discussion started: 2 June 2025

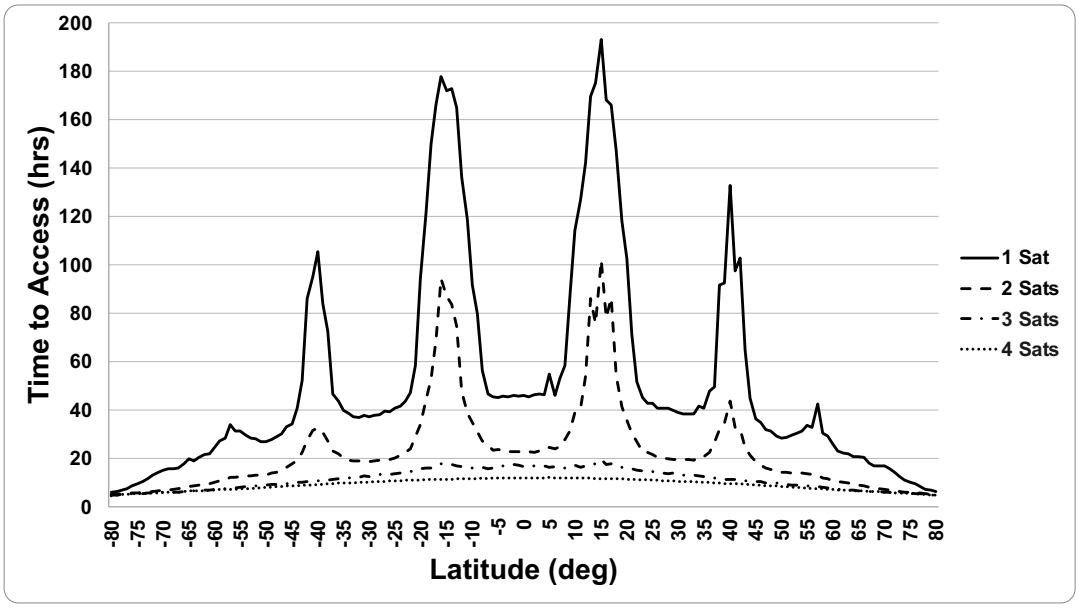

Figure 25. The median Time To Access (TTA) and number of satellites are key factors constraining the revisit intervals for a given observational target at a given latitude. In practice, the achievable revisit interval for mapping large regions depends on TTA and other factors such as cloud cover and the spatial distribution of target areas (e.g., dense collections of images over large regions can result in tasking conflicts which increase the time required to observe them).

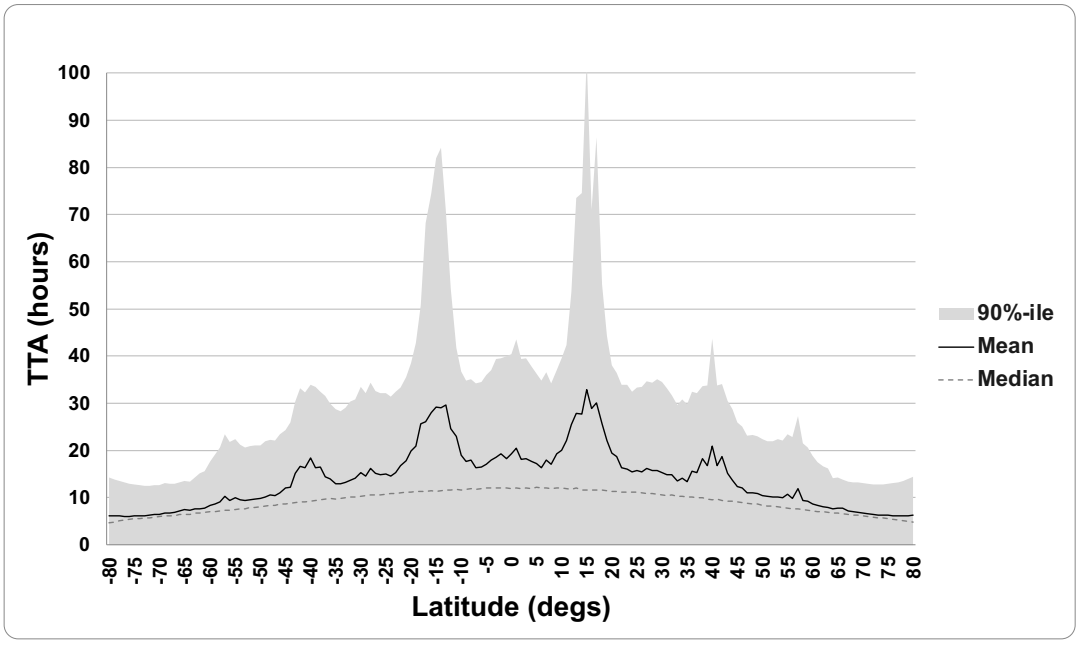

Figure 26. The median, mean, and 90 percentile time to access (TTA) for a constellation of four Tanager satellites indicating the ability to provide sub-daily sampling for isolated priority areas at mid latitudes.

https://doi.org/10.5194/egusphere-2025-2275
Preprint. Discussion started: 2 June 2025

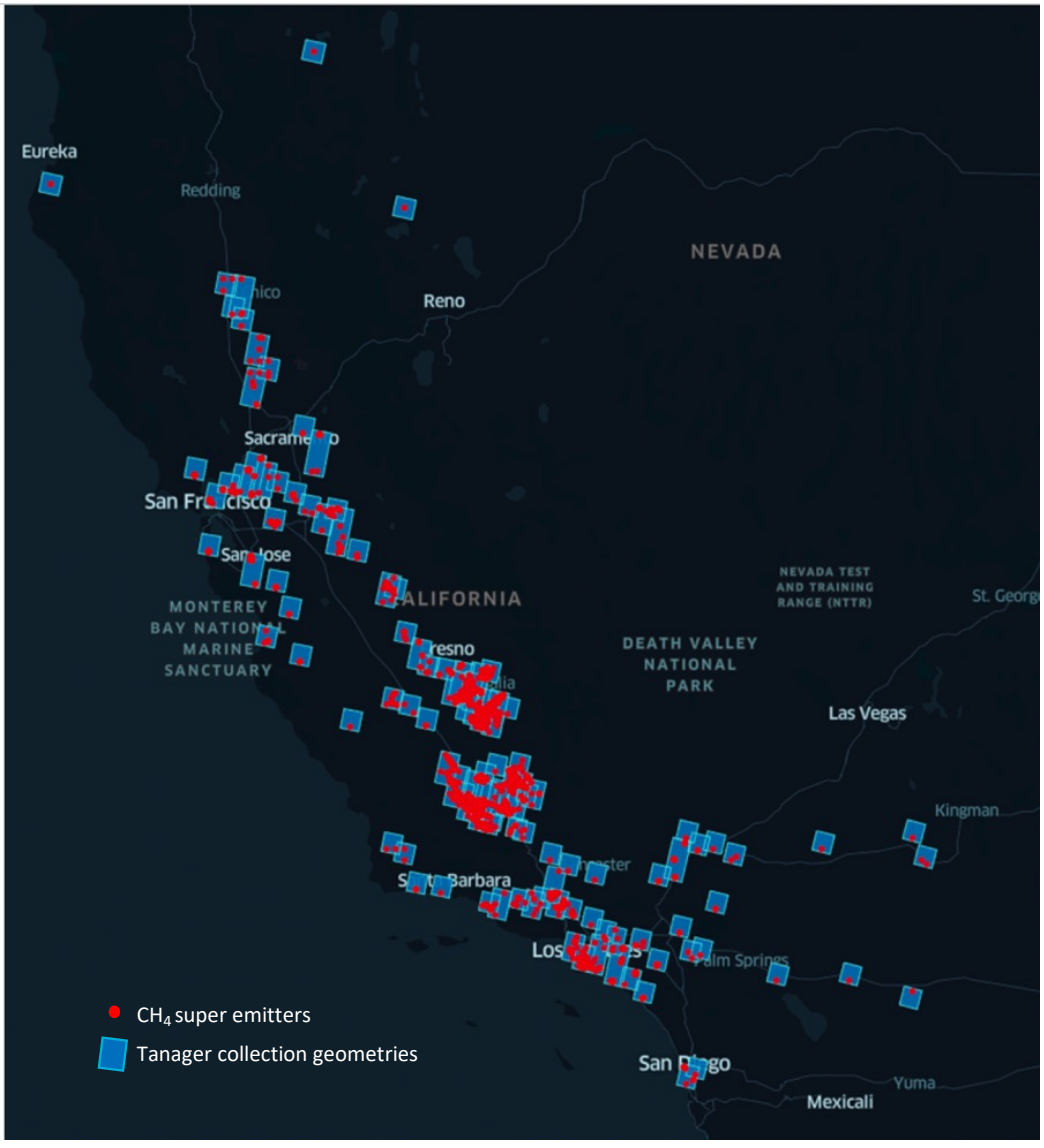

Figure 27. Example of the coverage capabilities of a four Tanager constellation for monitoring priority methane emitting areas in California. This simulation aggregated the 3,571 AOIs into 112 collection geometries to monitor previously detected methane super emitters across California. The simulation shows that 4 Tanager satellites can observe 93% of the targets on a biweekly cadence and 100% of the targets on a monthly cadence. For a subset of targets, sub-daily sampling is possible.

However, TTA isn't the only factor that determines revisit interval. When mapping large areas through repeated tasking of high-resolution satellites, cloud cover and the spatial distribution of AOI's can significant impact the achievable sample frequency. Attempting to map a region with a spatially dense set of tasking targets can lead to conflicts which increase the time required to observe them. In such cases, designing efficient monitoring strategies

https://doi.org/10.5194/egusphere-2025-2275
Preprint. Discussion started: 2 June 2025

requires iteratively evaluating different scenarios. Figure 27 illustrates one such scenario, mapping a notional tasking deck within the state of California with four Tanager satellites. A simulation was run that models the number of successful observations for specified monitoring cadences and AOIs across California as well as the satellite orbits and observational constraints. The simulation accounted for cloud-cover using a MODIS monthly cloud cover model. If an observation during an interval window was deemed cloudy, then collection attempts would continue until either the observation was successful, or the window expired. The simulation also accounted for seasonal variations in solar zenith angle. Simulations were run using Planet's internal code for calculating access opportunities and collection optimizations. The four Tanager satellites were modeled in a 406 km altitude, sun-synchronous orbit. We used an average instrument swath width of 18.6 km and limited off-nadir angles to 35 degrees. Each observation involves along-track (and in many cases, cross-track) pointing to provide varying degrees of ground-motion compensation. The simulation used High Sensitivity imaging mode that is predicted to deliver ≤100 kg CH_4/h 90% Probability of Detection for the reference observation. This scenario is based on the union of all methane plumes detected by aircraft surveys of this region between 2016 and 2023 and the GFEI for methane emissions, which resulted in 3,571 AOIs. The simulation included optimizations to combine AOIs such that a minimum number of areas need to be imaged to cover the largest number of targets. This optimization aggregated the 3,571 AOIs into 112 collection geometries (blue polygons) to monitor previously detected methane super emitters across California (red points). Standard priority levels were used in the simulation. The simulation shows that four Tanager satellites can observe 93% of the targets on a biweekly cadence and 100% of the targets on a monthly cadence. For a subset of targets, sub-daily sampling is possible. Note that using Standard and Medium sensitivity modes would provide broader spatial coverage and/or higher frequency cadences, at the expense of decreased sensitivity.

5 Summary

We have described the design and observational strategies of the Carbon Mapper emissions monitoring system and provided an initial validation of the performance of Planet's Tanager-1 satellite through coordinated field measurements. We also demonstrated a range of key functional capabilities that were exercised during commissioning spanning observation, plume detection, quantification and rapid reporting. These empirical results indicate that Carbon Mapper and on-orbit Tanager performance is meeting our performance requirements, laying the foundation for further operational scale-up as more satellites are launched. Future papers will provide additional details on Tanager calibration and validation procedures, additional quantitative demonstration of CH_4 estimation accuracy and probabilistic detection limits through blinded controlled release experiments, and further simulations of observing system completeness informed by actual operational experience.

The Carbon Mapper emission monitoring system is ultimately designed to detect, quantify and track 90% of the world's high emission CH_4 and CO_2 point sources. Meeting that target will likely require a constellation of 10 or more Tanager satellites, because of observing system completeness demands for increased spatial coverage and sample frequency. Meanwhile, the planned interim constellation of four Tanager satellites is predicted to deliver about 60% completeness for super-emitter detection globally and much higher completeness (approaching 100%) for selected regions. We estimate that this interim capability could enable the detection of about 56 $TgCH_4$/year in super-emitter emissions assuming that CH_4 point sources above 100 $kgCH_4$/h contribute 10%, 30%, 50% and 50%, respectively, to the agriculture, oil and gas, coal production and waste management sectors globally using bottom-up methane inventories for those sectors (Saunois *et al.* 2025). While those high emission point sources likely only constitute about 20% of the global anthropogenic methane budget, they are also good candidates for expedited mitigation given those super emitters would be limited to a few thousand sites globally (compared to the millions of facilities that contribute the remaining methane flux including distributed area sources). Given the Global Methane Pledge of reducing methane emissions by 30% by 2030, the ability to expedite action on mitigating methane super emitters could be an important component of the broader portfolio of mitigation programs this decade.

Beyond offering mitigation guidance for methane super-emitters, the Carbon Mapper emissions monitoring system is designed to improve quantitative understanding awareness of high emission CH_4 and CO_2 point sources at 30 meter resolution for key regions around the globe through improved monitoring of the cloudy tropics, high latitudes and offshore oil and gas infrastructure – areas that have traditionally been challenging to observe. In doing so, our system serves as a key component in the growing multi-scale, tiered observing system for CH_4 and CO_2 emissions including other point source imagers as well as area flux mapping satellites.

https://doi.org/10.5194/egusphere-2025-2275
Preprint. Discussion started: 2 June 2025

Data Availability

To aid in expanded global awareness and data accessibility, Carbon Mapper publishes CH_4 and CO_2 data for all plumes detected by our system as quickly as 30 days following each observation, including quality-controlled retrieval outputs, plume images, coordinates, emission rates, uncertainties and attribution to source type. All Carbon Mapper CH_4 and CO_2 data is available for viewing and download via the Carbon Mapper public data portal (https://data.carbonmapper.org) and API (https://api.carbonmapper.org/api/v1/docs). Carbon Mapper documents including our Data Product Guide, Algorithm Theoretical Basis Documents, and Quality Control Description Document are available in the Technical Resources section of our website (https://carbonmapper.org/resources/technical-resources). Additionally, rapid access (within 72 hours) to Carbon Mapper quick-look methane products derived from Tanager is available from Planet for subscribers. Data from the controlled release tests referenced in this paper is available at the following repository https://doi.org/10.25740/qh001qt3946.

Author Contributions

RD conceptualized and acquired funding for this work. RD, JN, MK, JG, JM, PG, and RG supervised key program elements. RD, DC, AA, KH, AD, TS, JK, KO, AT, SZ, LS, MG, RN, GB, DRT, and KR developed methodologies and implemented analysis. DJ, ME, FR, TA, AB, and EAK provided validation through independent aircraft under-flights and controlled release experiments. RD and DC wrote the draft manuscript, and all coauthors contributed to review and editing.

Competing interests

The authors declare that they have no conflict of interest.

Acknowledgements

Carbon Mapper acknowledges the generous support of our philanthropic donors particularly the High Tide Foundation, Grantham Foundation for the Protection of the Environment, Bloomberg Philanthropies, and other contributors. Portions of this work were performed at the Jet Propulsion Laboratory, California Institute of Technology, under a contract with the National Aeronautics and Space Administration (80NM0018D0004). The Carbon Mapper emissions monitoring system benefited from over a decade of research and technology development enabled by sustained support of NASA's Earth Science Division including the Carbon Monitoring System and airborne science programs. We thank the operations and data platform teams at Planet and Carbon Mapper for their efforts in managing Tanager observations and data delivery. Finally, we thank the management and staff of JPL and Planet for their support in establishing the unique public-private partnership that has underpinned this work.

References

Ayasse, A.K., Thorpe, A.K., Cusworth, D.H., Kort, E.A., Negron, A.G., Heckler, J., Asner, G.P., Duren, R.M. Methane remote sensing and emission quantification of offshore shallow water oil and gas platforms in the Gulf of Mexico, *Environ. Res. Lett.* **17** 084039 https://iopscience.iop.org/article/10.1088/1748-9326/ac8566/meta, 2022.

Ayasse, A. K., Cusworth, D., O'Neill, K., Fisk, J., Thorpe, A. K., and Duren, R.: Performance and sensitivity of column-wise and pixel-wise methane retrievals for imaging spectrometers, Atmos. Meas. Tech., 16, 6065–6074, https://doi.org/10.5194/amt-16-6065-2023, 2023.

Biener, K.J., Negron, A.G., Kort,E.A., Ayasse, A.K., Chen, Y., MacLean, J., and McKeever. J., *Environmental Science & Technology*, *58* (11), 4948-4956, DOI: 10.1021/acs.est.3c08066, 2024.

Bruegge, C.J., Arnold, G.T., Czapla-Myers, J., Dominguez, R., Helmlinger, M.C., Thompson, D.R., Van den Bosch, J. and Wenny, B.N. Vicarious calibration of eMAS, AirMSPI, and AVIRIS sensors during FIREX-AQ. *IEEE Transactions on Geoscience and Remote Sensing*, *59*(12), 2021.

Byrne, B., Baker, D. F., Basu, S., Bertolacci, M., Bowman, K. W., Carroll, D., Chatterjee, A., Chevallier, F., Ciais, P., Cressie, N., Crisp, D., Crowell, S., Deng, F., Deng, Z., Deutscher, N. M., Dubey, M. K., Feng, S., García, O. E., Griffith, D. W. T., Herkommer, B., Hu, L., Jacobson, A. R., Janardanan, R., Jeong, S., Johnson, M. S., Jones, D. B.

https://doi.org/10.5194/egusphere-2025-2275
Preprint. Discussion started: 2 June 2025

A., Kivi, R., Liu, J., Liu, Z., Maksyutov, S., Miller, J. B., Miller, S. M., Morino, I., Notholt, J., Oda, T., O'Dell, C. W., Oh, Y.-S., Ohyama, H., Patra, P. K., Peiro, H., Petri, C., Philip, S., Pollard, D. F., Poulter, B., Remaud, M., Schuh, A., Sha, M. K., Shiomi, K., Strong, K., Sweeney, C., Té, Y., Tian, H., Velazco, V. A., Vrekoussis, M., Warneke, T., Worden, J. R., Wunch, D., Yao, Y., Yun, J., Zammit-Mangion, A., and Zeng, N.: National CO_2 budgets (2015–2020) inferred from atmospheric CO_2 observations in support of the global stocktake, Earth Syst. Sci. Data, 15, 963–1004, https://doi.org/10.5194/essd-15-963-2023, 2023.

CARB, California Air Resources Board, Summary Report of the 2020, 2021, and 2023 Airborne Methane Plume Mapping Studies, 2024, https://ww2.arb.ca.gov/resources/documents/summary-report-2020-2021-and-2023-airborne-methane-plume-mapping-studies?keywords=2025

CDPHE, Colorado Department of Public Health and the Environment, Aircraft Methane Plume Mapping Summary Report, 2024, https://cdphe.colorado.gov/greenhouse-gas-monitoring-projects-reports-and-data

Crisp, D., R.M Atlas, F.-M Breon, L.R Brown, J.P Burrows, P Ciais, B.J Connor, S.C Doney, I.Y Fung, D.J Jacob, C.E Miller, D O'Brien, S Pawson, J.T Randerson, P Rayner, R.J Salawitch, S.P Sander, B Sen, G.L Stephens, P.P Tans, G.C Toon, P.O Wennberg, S.C Wofsy, Y.L Yung, Z Kuang, B Chudasama, G Sprague, B Weiss, R Pollock, D Kenyon, S Schroll, The Orbiting Carbon Observatory (OCO) mission, Advances in Space Research, Volume 34, Issue 4, Pages 700-709, ISSN 0273-1177, https://doi.org/10.1016/j.asr.2003.08.062, 2004.

Cusworth, D.H., Duren, R.M., Thorpe, A.K., Olson-Duvall, W., Heckler, J., Chapman, J.W., Eastwood, M.L., "Intermittency of Large Methane Emitters in the Permian Basin." *Environmental Science & Technology Letters* 8 (7): 567–73. https://doi.org/10.1021/acs.estlett.1c00173, 2021a.

Cusworth, D.H., Duren, R.M., Thorpe, A.K., Eastwood, M.L., Green, R.O., Dennison, P.E., Frankenberg, C., Heckler, J.W., Asner, G.P., and Miller, C.E.,"Quantifying Global Power Plant Carbon Dioxide Emissions With Imaging Spectroscopy." *AGU Advances* 2 (2). https://doi.org/10.1029/2020AV000350, 2021b.

Cusworth, D.H., Thorpe, A.K., Ayasse, A.K., Stepp, D., Heckler, J., Asner, G.P., Miller, C.E., Chapman, J.W., Eastwood, M.L., Green, R.O., Hmiel, B., Lyon, D., and Duren, R.M. Strong methane point sources contribute a disproportionate fraction of total emissions across multiple basins in the U.S., *Proc. Natl Acad. Sci.* 119 (38) https://doi.org/10.1073/pnas.2202338119, 2022.

Cusworth, D.H., Duren, R.M., et al, Quantifying Methane Emissions from United States Landfills, *Science* ***383****,1499-1504(2024).DOI:10.1126/science.adi7735, 2024.*

Duren, R.M., Thorpe, A.K., Foster, K.T., Rafiq, T., Hopkins, F.M., et al. "California's Methane Super emitters." *Nature* 575 (7781): 180–84. https://doi.org/10.1038/s41586-019-1720-3, 2019.

El Abbadi,S.H., Chen, Z., Burdeau, P.M., Rutherford, J.S., Chen, Y., Zhang Z., Sherwin, E.D., and Brandt, A.R., *Environmental Science & Technology 58* (22), 9591-9600 DOI: 10.1021/acs.est.4c02439, 2024.

Eldering, A., Taylor, T. E., O'Dell, C. W., and Pavlick, R.: The OCO-3 mission: measurement objectives and expected performance based on 1 year of simulated data, Atmos. Meas. Tech., 12, 2341–2370, https://doi.org/10.5194/amt-12-2341-2019, 2019.

Foote, M.D., Dennison, P.E., Thorpe, A.K., Thompson, D.R., Jongaramrungruang, S., Frankenberg, C., and Joshi, S.C., "Fast and Accurate Retrieval of Methane Concentration From Imaging Spectrometer Data Using Sparsity Prior." *IEEE Transactions on Geoscience and Remote Sensing* 58 (9): 6480–92. https://doi.org/10.1109/TGRS.2020.2976888, 2020.

Frankenberg, C., Platt, U., and Wagner, T."Iterative Maximum a Posteriori (IMAP)-DOAS for Retrieval of Strongly Absorbing Trace Gases: Model Studies for CH_4 and CO_2 Retrieval from near Infrared Spectra of SCIAMACHY Onboard." *Atmos. Chem. Phys.*, 14, 2005.

https://doi.org/10.5194/egusphere-2025-2275
Preprint. Discussion started: 2 June 2025

Frankenberg, C., Aben, I., Bergamaschi, P., Dlugokencky, E. J., van Hees, R., Houweling, S., van der Meer, P., Snel, R., and Tol, P., Global column-averaged methane mixing ratios from 2003 to 2009 as derived from SCIAMACHY: Trends and variability, *J. Geophys. Res.*, 116, D04302, doi:10.1029/2010JD014849, 2011.

Frankenberg, C., Thorpe, A.K., Thompson, D.R., Hulley, G., Kort, E.A., Vance, N., Borchardt, J., Krings, T., Gerilowski, K., Sweeney, C. and Conley, S., Airborne methane remote measurements reveal heavy-tail flux distribution in Four Corners region. *Proceedings of the national academy of sciences*, *113*(35), 2016.

Frankenberg, C., Bar-On, Y. M., Yin, Y., Wennberg, P. O., Jacob, D. J., & Michalak, A. M. Data drought in the humid tropics: How to overcome the cloud barrier in greenhouse gas remote sensing. *Geophysical Research Letters, 51, e2024GL108791. https://doi.org/10.1029/*, 2024.

Gorchov Negron,A.M., et al, Excess methane emissions from shallow water platforms elevate the carbon intensity of US Gulf of Mexico oil and gas production, *Proc. Natl. Acad. Sci. U.S.A. 120 (15) e2215275120, https://doi.org/10.1073/pnas.2215275120 (2023).*

Green, R.O., *et al*., "Airborne Visible/Infrared Imaging Spectrometer 3 (AVIRIS-3)," *2022 IEEE Aerospace Conference (AERO)*, Big Sky, MT, USA, pp. 1-10, doi: 10.1109/AERO53065.2022.9843565, 2022.

Hu, H., Landgraf, J., Detmers, R., Borsdorff, T., Aan de Brugh, J., Aben, I., et al. Toward global mapping of methane with TROPOMI: First results and intersatellite comparison to GOSAT. *Geophysical Research Letters*, 45, 3682–3689. https://doi.org/10.1002/2018GL077259, 2018.

Jacob, Daniel J., Alexander J. Turner, Joannes D. Maasakkers, Jianxiong Sheng, Kang Sun, Xiong Liu, Kelly Chance, Ilse Aben, Jason McKeever, and Christian Frankenberg. 2016. "Satellite Observations of Atmospheric Methane and Their Value for Quantifying Methane Emissions." *Atmospheric Chemistry and Physics* 16 (22): 14371–96. https://doi.org/10.5194/acp-16-14371-2016.

Jacob, D. J., Varon, D. J., Cusworth, D. H., Dennison, P. E., Frankenberg, C., Gautam, R., Guanter, L., Kelley, J., McKeever, J., Ott, L. E., Poulter, B., Qu, Z., Thorpe, A. K., Worden, J. R., and Duren, R. M.Quantifying methane emissions from the global scale down to point sources using satellite observations of atmospheric methane. *Atmos. Chem. Phys.* https://doi.org/10.5194/acp-2022-246, 2022.

Kayrros Methane Watch, retrieved April 5, 2025, https://methanewatch.kayrros.com/

Kim, J., Cusworth, D. H., Ayasse, A. K., Howell, K., O'Neill, K., & Duren, R. M. Performance of airborne imaging spectrometers for carbon dioxide detection and emission quantification. *Journal of Geophysical Research: Atmospheres*, 130, e2024JD042755. https://doi.org/10.1029/2024JD042755, 2025.

Lauvaux, T., Giron, C., Mazzolini, M., d'Aspremont, A., Duren, R., Cusworth, D., Shindell, D., Ciais, P. Global assessment of oil and gas methane ultra-emitters, *Science*, 2 375, 6580 557-561 https://www.science.org/doi/10.1126/science.abj4351, 2022.

Miller, C., C., Roche, S., Wilzewski, J. S., Liu, X., Chance, K., Souri, A. H., Conway, E., Luo, B., Samra, J., Hawthorne, J., Sun, K., Staebell, C., Chulakadabba, A., Sargent, M., Benmergui, J. S., Franklin, J. E., Daube, B. C., Li, Y., Laughner, J. L., Baier, B. C., Gautam, R., Omara, M., and Wofsy, S. C.: Methane retrieval from MethaneAIR using the CO_2 proxy approach: a demonstration for the upcoming MethaneSAT mission, Atmos. Meas. Tech., 17, 5429–5454, https://doi.org/10.5194/amt-17-5429-2024, 2024.

Mouroulis, P., Robert O. Green, "Review of high fidelity imaging spectrometer design for remote sensing," Opt. Eng. 57(4), 040901, doi: 10.1117/1.OE.57.4.040901, 2018.

Naus, S., Maasakkers, J.D., Gautam, R., Omara, M., Stikker, R., Veenstra, A.K., Nathan, B., Irakulis-Loitxate, I., Guanter, L., Pandey, S., Girard, M., Lorente, A., Borsdorff, T., and Aben, I., *Environmental Science & Technology 57* (48), 19545-19556 DOI: 10.1021/acs.est.3c04746, 2023.

https://doi.org/10.5194/egusphere-2025-2275
Preprint. Discussion started: 2 June 2025

Nassar, R., Mastrogiacomo, J-P., Bateman-Hemphill, W., McCracken, C., MacDonald, C.G., Hill, T., O'Dell, C.W., Kiel, M., Crisp, D., Advances in quantifying power plant CO2 emissions with OCO-2, *Remote Sensing of Environment,* Volume 264, 112579, ISSN 0034-4257, https://doi.org/10.1016/j.rse.2021.112579, 2021.

Nesser, H., Jacob, D. J., Maasakkers, J. D., Lorente, A., Chen, Z., Lu, X., Shen, L., Qu, Z., Sulprizio, M. P., Winter, M., Ma, S., Bloom, A. A., Worden, J. R., Stavins, R. N., and Randles, C. A.: High-resolution US methane emissions inferred from an inversion of 2019 TROPOMI satellite data: contributions from individual states, urban areas, and landfills, Atmos. Chem. Phys., 24, 5069–5091, https://doi.org/10.5194/acp-24-5069-2024, 2024.

Pandey, S., R. Gautam, S. Houweling, H.D. van der Gon, P. Sadavarte, T. Borsdorff, O. Hasekamp, J. Landgraf, P. Tol, T. van Kempen, R. Hoogeveen, R. van Hees, S.P. Hamburg, J.D. Maasakkers, & I. Aben, Satellite observations reveal extreme methane leakage from a natural gas well blowout, Proc. Natl. Acad. Sci. U.S.A. 116 (52) 26376-26381, https://doi.org/10.1073/pnas.1908712116, 2019.

Saunois, M., Martinez, A., Poulter, B., Zhang, Z., Raymond, P., Regnier, P., Canadell, J. G., Jackson, R. B., Patra, P. K., Bousquet, P., Ciais, P., Dlugokencky, E. J., Lan, X., Allen, G. H., Bastviken, D., Beerling, D. J., Belikov, D. A., Blake, D. R., Castaldi, S., Crippa, M., Deemer, B. R., Dennison, F., Etiope, G., Gedney, N., Höglund-Isaksson, L., Holgerson, M. A., Hopcroft, P. O., Hugelius, G., Ito, A., Jain, A. K., Janardanan, R., Johnson, M. S., Kleinen, T., Krummel, P., Lauerwald, R., Li, T., Liu, X., McDonald, K. C., Melton, J. R., Mühle, J., Müller, J., Murguia-Flores, F., Niwa, Y., Noce, S., Pan, S., Parker, R. J., Peng, C., Ramonet, M., Riley, W. J., Rocher-Ros, G., Rosentreter, J. A., Sasakawa, M., Segers, A., Smith, S. J., Stanley, E. H., Thanwerdas, J., Tian, H., Tsuruta, A., Tubiello, F. N., Weber, T. S., van der Werf, G., Worthy, D. E., Xi, Y., Yoshida, Y., Zhang, W., Zheng, B., Zhu, Q., Zhu, Q., and Zhuang, Q.: Global Methane Budget 2000–2020, Earth Syst. Sci. Data, 17, 1873–1958, https://doi.org/10.5194/essd-17-1873-2025, 2025.

Scarpelli, T., R., Cusworth, D.H., Duren, R.M., Kim, J., Heckler, J., Asner, G.P., Thoma, E., Krause, M.J., Heins, D., and Thorneloe, S., *Environmental Science & Technology 58* (49), 21545-21556 DOI: 10.1021/acs.est.4c07572, 2024.

Sherwin, E.D., Rutherford, J.S., Zhang, Z. *et al.* US oil and gas system emissions from nearly one million aerial site measurements. *Nature* **627**, 328–334, https://doi.org/10.1038/s41586-024-07117-5, 2024.

Thompson, D. R., I. Leifer, H. Bovensmann, M. Eastwood, M. Fladeland, C. Frankenberg, K. Gerilowski, et al. "Real-Time Remote Detection and Measurement for Airborne Imaging Spectroscopy: A Case Study with Methane." *Atmospheric Measurement Techniques* 8 (10): 4383–97. https://doi.org/10.5194/amt-8-4383-2015, 2015.

Thompson, D. R., Thorpe, A. K., Frankenberg, C., Green, R. O., Duren, R., Guanter, L., ... & Ungar, S.. Space-based remote imaging spectroscopy of the Aliso Canyon CH4 superemitter. *Geophysical Research Letters*, *43*(12), 2016.

Thompson, D. R., V. Natraj, R. O. Green, M. C. Helmlinger, B-C Gao, and M. L. Eastwood. "Optimal estimation for imaging spectrometer atmospheric correction." *Remote sensing of environment* 216, 2018.

Thompson, D. R., R. O. Green, C. Bradley, P. G. Brodrick, N. Mahowald, E. Ben Dor, M. Bennett et al. "On-orbit calibration and performance of the EMIT imaging spectrometer." *Remote Sensing of Environment* 303: 113986, 2024.

Thorpe, A.,K., Frankenberg, C., Thompson, D.R., Duren, R.M., Aubrey, A.D., Bue, B.D., Green, R.O., et al. "Airborne DOAS Retrievals of Methane, Carbon Dioxide, and Water Vapor Concentrations at High Spatial Resolution: Application to AVIRIS-NG." *Atmospheric Measurement Techniques* 10 (10): 3833–50. https://doi.org/10.519₄/amt-10-3833-2017, 2017.

Thorpe, A.K., *et al.,* Attribution of individual methane and carbon dioxide emission sources using EMIT observations from space.*Sci. Adv.***9**,eadh2391(2023).DOI:10.1126/sciadv.adh2391

https://doi.org/10.5194/egusphere-2025-2275
Preprint. Discussion started: 2 June 2025

Turner, A. J., Jacob, D. J., Wecht, K. J., Maasakkers, J. D., Lundgren, E., Andrews, A. E., Biraud, S. C., Boesch, H., Bowman, K. W., Deutscher, N. M., Dubey, M. K., Griffith, D. W. T., Hase, F., Kuze, A., Notholt, J., Ohyama, H., Parker, R., Payne, V. H., Sussmann, R., Sweeney, C., Velazco, V. A., Warneke, T., Wennberg, P. O., and Wunch, D.: Estimating global and North American methane emissions with high spatial resolution using GOSAT satellite data, Atmos. Chem. Phys., 15, 7049–7069, https://doi.org/10.5194/acp-15-7049-2015, 2015.

United Nations, 2015, Paris Agreement, https://unfccc.int/process-and-meetings/the-paris-agreement

United Nations, 2016, Kigali Amendment to the Montreal Protocol, https://treaties.un.org/doc/Treaties/2016/10/20161015%2003-23%20PM/Ch_XXVII-2.f-English%20and%20French.pdf

United Nations, 2023, Global Methane Pledge, https://www.globalmethanepledge.org/resources/global-methane-pledge

UNEP, 2020, Oil and Gas Methane Partnership 2.0, https://www.ogmpartnership.org/

United States Environmental Protection Agency, 2024a, 40 CFR Part 60 - Standards of Performance for New, Reconstructed, and Modified Sources and Emissions Guidelines for Existing Sources: Oil and Natural Gas Sector, EPA–HQ–OAR–2021–0317, https://www.federalregister.gov/d/2024-13206

United States Environmental Protection Agency, 2024b, 40 CFR Part 98 —Mandatory Greenhouse Gas Reporting, Subpart W—Petroleum and Natural Gas Systems, https://www.ecfr.gov/current/title-40/part-98/subpart-W

Worden, J. R., Cusworth, D. H., Qu, Z., Yin, Y., Zhang, Y., Bloom, A. A., Ma, S., Byrne, B. K., Scarpelli, T., Maasakkers, J. D., Crisp, D., Duren, R., and Jacob, D. J.: The 2019 methane budget and uncertainties at 1° resolution and each country through Bayesian integration Of GOSAT total column methane data and a priori inventory estimates, Atmos. Chem. Phys., 22, 6811–6841, https://doi.org/10.5194/acp-22-6811-2022, 2022.

Zandbergen, S.R., Duren, R., Giuliano, P., Green, R.O., Haag, J.M., Moore, L.B., Shaw, L., and Mouroulis, P., "Optical design of the Carbon Plume Mapper (CPM) imaging spectrometer", Proc. SPIE 12235, Imaging Spectrometry XXV: Applications, Sensors, and Processing, 1223505 (30 September 2022); https://doi.org/10.1117/12.2633767, 2022.

Zandbergen, S.R., Shaw, L., Klein, C., Thompson, D.R., Green, R.O., Duren, R., Gibson, M., Nazaryan, H., Smith, C., Cubanski, B., Giuliano, P., Haag, J.M., and Pritchett, C., "Preliminary alignment, characterization, and comparison of next generation carbon mapping imaging spectrometers", Proc. SPIE 12688, Imaging Spectrometry XXVI: Applications, Sensors, and Processing, 126880C (30 October 2023); https://doi.org/10.1117/12.2678614, 2023.

Zou, M., Xiong, X., Saitoh, N., Warner, J., Zhang, Y., Chen, L., Weng, F., and Fan, M.: Satellite observation of atmospheric methane: intercomparison between AIRS and GOSAT TANSO-FTS retrievals, Atmos. Meas. Tech., 9, 3567–3576, https://doi.org/10.5194/amt-9-3567-2016, 2016.